Chapter in **Advancing Astrophysics with the SKA – II**

Small-scale Magnetic Fields in the Milky Way and Nearby Galaxies

Yik Ki Ma [*,1] Amit Seta [*,2] Aritra Basu [3,1] Sebastian Hutschenreuter [4] Marco Padovani [5] Georgia V. Panopoulou [6] Jeroen M. Stil [7] Craig S. Anderson [2] Lucia Armillotta [8] Jennifer Y. H. Chan [9,10,11] Marijke Haverkorn [12] Roland M. Crocker [2] Timea O. Kovacs [13] Sunil Malik [14] S. A. Mao [1] and Kierra J. Weatherhead [7]

[*] *These authors jointly co-lead the Chapter and contributed equally to the work.*

[1] *Max-Planck-Institut für Radioastronomie, Auf dem Hügel 69, 53121 Bonn, Germany*

[2] *Research School of Astronomy & Astrophysics, Australian National University, Canberra, ACT 2611, Australia*

[3] *Thüringer Landessternwarte, Sternwarte 5, 07778 Tautenburg, Germany*

[4] *University of Vienna, Department of Astrophysics, Türkenschanzstraße 17, 1180 Vienna, Austria*

[5] *INAF-Osservatorio Astrofisico di Arcetri, Largo E. Fermi 5, 50125 Firenze, Italy*

[6] *Department of Space, Earth and Environment, Chalmers University of Technology, 412 93, Göteborg, Sweden*

[7] *Department of Physics and Astronomy, The University of Calgary, 2500 University Drive NW, Calgary, AB T2N 1N4, Canada*

[8] *University of Florence, Department of Physics and Astronomy, via G. Sansone 1, 50019 Sesto Fiorentino, Firenze, Italy*

[9] *Department of Physics and Astronomy, Oberlin College, Oberlin, OH 44074, USA*

[10] *Dunlap Institute for Astronomy and Astrophysics, 50 St. George Street, Toronto, Ontario, M5S 3H4, Canada*

[11] *Canadian Institute for Theoretical Astrophysics, University of Toronto, 60 St George St, Toronto, ON M5S 3H8, Canada*

[12] *Department of Astrophysics/IMAPP, Radboud University, PO Box 9010, 6500 GL Nijmegen, The Netherlands*

[13] *Max-Planck-Institut für Astronomie, Königstuhl 17, 69117 Heidelberg, Germany*

[14] *Departamento de Física de la Tierra y Astrofísica & IPARCOS-UCM, Universidad Complutense de Madrid, 28040 Madrid, Spain*

E-mail: ykma@mpifr-bonn.mpg.de, amit.seta@anu.edu.au

Magnetic fields in galaxies span decades in physical scale, from the coherent magnetic fields on galactic scales (> kpc) to the random magnetic fields from 100 pc to the resistive scale of the galactic plasma (i.e. $\sim 10^6$ cm). While many radio studies to date have placed more emphasis on the large-scale galactic magnetic fields than the small-scale counterparts, the emerging SKA will greatly facilitate accurate, detailed studies of the small-scale ($\lesssim 100$ pc) galactic magnetic fields. In this Chapter, we highlight the importance of understanding the small-scale galactic magnetic fields in furthering our understanding of star formation, galaxy evolution, and the fundamental physics of magnetohydrodynamics. Furthermore, we discuss some open questions in the research field and outline several possible large observation programmes with the SKA Array Assembly 4 (AA4).

1 Introduction

Magnetic fields are a dynamically important component of the interstellar medium (ISM) of galaxies, as they play a crucial role in star formation (Pattle et al., 2023), regulate the propagation of cosmic rays (Ruszkowski and Pfrommer, 2023), and influence gas morphology, distribution, and flow (Planck Collaboration et al., 2016). The magnetic energy density in the Milky Way ($\sim 1\,\mathrm{eV\,cm^{-3}}$) is comparable to the thermal, turbulent kinetic, and cosmic ray energy densities, making it an energetically significant component of the ISM. However, the properties of ISM magnetic fields, in both the Milky Way and external galaxies, are not well known. This is particularly true on small scales ($\lesssim 100\,\mathrm{pc}$), making it difficult to fully understand their role in star formation and galaxy evolution – two outstanding questions in modern astrophysics. This Chapter discusses the current theoretical and observational understanding of these small-scale magnetic fields in the Milky Way and nearby galaxies and describes the transformative science that will be enabled by the SKA in its Array Assembly 4 (AA4).

Magnetic fields are directly connected to velocity fields, and for disk galaxies, this includes both the more systematic differential rotation and chaotic, random, turbulent motions. Turbulence in the ISM of galaxies is driven by a variety of mechanisms operating across a range of scales. On smaller scales ($\lesssim 100\,\mathrm{pc}$), stellar feedback processes (namely, protostellar jets, stellar outflows, and supernova explosions; each could be at a very different scale within $\sim 100\,\mathrm{pc}$) are the primary drivers of turbulence (Elmegreen and Scalo, 2004). On larger, kpc-scales, shear from galactic differential rotation and gravitational instabilities also introduce turbulence (Krumholz et al., 2018). Energetically, supernova explosions are the most powerful drivers of ISM turbulence; thus, the typical driving scale of turbulence, ℓ_{turb}, is often taken to be the average supernova remnant size, approximately 100 pc (e.g., see Gent et al., 2013). Based on ℓ_{turb}, galactic magnetic fields are typically divided into two types: large-scale, coherent (or "regular") fields with length scales of a few kpc (B_{reg}; usually approximately aligned with the spiral arms or interarm regions; see, e.g., Fletcher et al., 2011; Beck, 2015), and small-scale, turbulent fields on scales of $\lesssim 100\,\mathrm{pc}$ (b_{iso} and b_{ani}; see below). We emphasise that magnetic fields in galaxies are inherently multi-scale with power at a range of scales (usually characterised by a power spectrum). When distinguishing between small- and large-scale components, we primarily refer to their respective correlation scales; the range of spatial scales over which power is distributed can still overlap between the two components. This work primarily focuses on the science of the small-scale fields as probed by the SKA and its precursors.

Magnetic fields in the early Universe ($\approx 10^{-10}\,\mu\mathrm{G}$) and in protogalaxies ($\approx 10^{-4}\,\mu\mathrm{G}$) are significantly weaker (Subramanian, 2016) than those observed in the present day galaxies (1–10 μG, Beck, 2016). This amplification and subsequent maintenance of magnetic fields are due to dynamos, the process of converting turbulent kinetic energy into magnetic energy (Ruzmaikin et al., 1988; Brandenburg and Subramanian, 2005; Rincon, 2019; Shukurov and Subramanian, 2021). Based on scale, dynamos are classified into two types: large- and small-scale dynamos. The small-scale dynamo (also referred to as the fluctuation dynamo) converts turbulent kinetic energy into magnetic energy on short eddy-turnover timescales ($\approx 10^7$ yr) at scales smaller than the turbulent driving scale of $\approx 100\,\mathrm{pc}$ (Kazantsev, 1968; Schekochihin et al., 2004; Haugen et al., 2004; Seta et al., 2020; Seta and Federrath, 2021). The resultant galactic magnetic field component is commonly referred to as

the isotropic turbulent magnetic field ($b_{\rm iso}$). Such magnetic fields can be further enhanced and ordered by the large-scale dynamo (also referred to as the mean-field or α–Ω dynamo), which operates on galactic rotation timescales ($\approx 10^8$ yr) and over length scales of a few kpc, due to the combined effects of density stratification along the disk height (α) and differential rotation (Ω) (Ruzmaikin et al., 1988; Beck et al., 1996; Brandenburg and Subramanian, 2005; Rincon, 2019; Shukurov and Subramanian, 2021). The large-scale field generated by the large-scale dynamo can also be tangled by ISM turbulence, further producing small-scale random fields (see Appendix A in Seta et al. 2018 and Sec. 4.1 in Seta and Federrath 2020). Meanwhile, spiral shocks, differential rotation, and gaseous shearing motion can compress the small-scale turbulent magnetic field (Laing, 1980), causing the resulting magnetic fields to follow a single orientation (but can flip in direction by 180°). This magnetic component of galaxies is referred to as the anisotropic turbulent / ordered random / striated magnetic field ($b_{\rm ani}$; see e.g. Jaffe et al., 2010; Jansson and Farrar, 2012; Haverkorn, 2015; Beck, 2016; Kierdorf et al., 2020; Ma et al., 2025). Here, we primarily discuss how radio polarisation observations can help us understand the properties of the small-scale fields, the small-scale dynamo, and their connection with the galactic ecosystem.

This Chapter is structured as follows. In Sec. 2, we briefly summarise the observational probes of small-scale magnetic fields that one can employ with the SKA. In Sec. 3, we discuss the high-level scientific goals in this research area, and in Sec. 4, we explore the specific astrophysics questions that can be addressed with the SKA. Sec. 5 highlights the preparation works that the community ought to focus on in the coming years in the lead-up to the SKA (Sec. 5.1), describes in general the types of SKA observations that can benefit small-scale galactic magnetic field studies (Sec. 5.2), presents several prospective large observation programmes with the SKA AA4 (Sec. 5.3), and highlights multiple anticipated advancements beyond the radio wavelengths that synergise with our proposed science with SKA (Sec. 5.4).

2 Observing Galactic Small-scale Magnetic Fields

We provide a brief overview of the observational tracers of galactic small-scale magnetic fields that we will be able to utilise with the SKA. In addition, we highlight the key differences in the use of these tracers for the cases of the Milky Way and external galaxies. Furthermore, we point out how recent advancements have enabled direct comparisons between upcoming SKA results with the numerical simulations counterparts.

2.1 Overview of the Observational Tracers

2.1.1 Synchrotron Emission

Synchrotron emission is radiated by ultra-relativistic charged particles (primarily electrons, in an astrophysical context) subjected to magnetic fields, with the (intrinsic) linear polarisation plane being perpendicular to the magnetic field orientation (Rybicki and Lightman, 1979). Below, we separately discuss the two main components of the small-scale magnetic fields in galaxies (see also Jaffe et al., 2010; Haverkorn, 2015; Beck, 2016; Beck et al., 2019).

- *Anisotropic turbulent magnetic fields ($b_{\rm ani}$):* Despite the 180° flips in the magnetic field direction on small scales (believed to be $\lesssim 100$ pc), $b_{\rm ani}$ follows the same orientation on $\gtrsim$ kpc

scales. Thus, $b_{\rm ani}$ contributes significantly to the linearly polarised synchrotron emission seen in nearby galaxies (e.g. Beck et al., 2019; Kierdorf et al., 2020), and possibly also that in the Milky Way (Jansson and Farrar, 2012)[1]. The plane-of-sky component of $b_{\rm ani}$ is traced by the intrinsic B-vector (= E-vector + 90°) of the linearly polarised electromagnetic waves, while the strength ($|b_{\rm ani}|$) can be estimated by considering both the polarisation fraction of the emission and the equipartition magnetic field strength, followed by subtracting the $B_{\rm reg}$ contribution.

- *Isotropic turbulent magnetic fields ($b_{\rm iso}$):* In typical observations that cannot spatially resolve $b_{\rm iso}$ (i.e. spatial resolution poorer than $\approx$ 100 pc), the observed synchrotron emission will appear unpolarised due to the (wavelength-independent[2]) beam depolarisation effect. This results from the intrinsic polarisation position angle of the synchrotron emission within the beam volume being isotropic, hence yielding a net zero observed polarisation (see e.g. Beck, 2016, Sec. 3.5). However, high-spatial-resolution SKA observations of the diffuse synchrotron emission of the Milky Way (see Chapter by Sun et al., 2026) can have the prospect of recovering the linearly polarised emission from $b_{\rm iso}$, thereby resolving its structure. Regarding the magnetic field strength ($|b_{\rm iso}|$), the *total* intensity of the synchrotron emission can be used to estimate the *total* magnetic field strength. This requires the assumption of energy equipartition between magnetic fields and cosmic ray particles (with caveats; see Beck and Krause, 2005; Seta and Beck, 2019; Ponnada et al., 2024). Subsequently, with the subtraction of the contributions by the other magnetic components (namely $b_{\rm ani}$ and $B_{\rm reg}$; e.g. Beck and Berkhuijsen, 2025), the $|b_{\rm iso}|$ values can be obtained.

An intriguing aspect of synchrotron radiation relevant to the SKA is its circular polarisation (CP). Unlike linear polarisation, CP depends on all magnetic field components at the emission site (Pandya et al., 2016). It can also be generated through Faraday conversion, where linear polarisation is transformed into circular polarisation as the signal propagates through a magnetised plasma (e.g. Macquart and Melrose, 2000). Detecting CP, however, is observationally challenging due to its typically very low fractional levels and the strong systematic biases that can obscure such weak signals, challenges that the SKA's unprecedented sensitivity and polarimetric precision are well suited to address (Enßlin et al., 2017).

2.1.2 Synchrotron Polarisation Statistics

The diffuse synchrotron polarisation observations of the ISM, Galactic Centre, and extended objects such as large supernova remnants at high resolution, facilitated by SKA, can also be utilised to infer MHD turbulence characteristics. Many of the established techniques have been driven by previous large-scale radio polarisation surveys, such as the Southern Galactic Plane Survey (SGPS; Haverkorn et al., 2006) and the Canadian Galactic Plane Survey (CGPS; Taylor et al., 2003; Landecker et al., 2010). One approach is to apply the radio polarisation gradient technique to Stokes Q

[1]Note that the Jansson and Farrar (2012) formulation assumes that $b_{\rm ani}$ ("striated field" in their nomenclature) is proportional to $B_{\rm reg}$ in strength, with the two following the same orientation. Recent modelling works suggest that such striated field may not be required (Korochkin et al., 2025). However, we point out that $b_{\rm ani}$ need not be directly related to $B_{\rm reg}$ in strength or orientation (e.g. Beck et al., 2019).

[2]We exclude here the frequency-dependent nature of the beam size of typical radio observations.

and U maps (Gaensler et al., 2011; Burkhart et al., 2012), which can potentially constrain several MHD characteristics (e.g. the sonic Mach number, magnetic field strength, and Reynolds number). Alternatively, one can perform power spectrum analysis to the Galactic diffuse polarised emission (Stutz et al., 2014). Another approach was recently discussed in Malik et al. (2023), based on the relative anisotropy of the global correlation functions constructed using the Stokes parameters as $I + Q$ and $I - Q$, referred to as the Y-parameter. To develop this approach, synthetic synchrotron maps from MHD turbulence data cubes having various plasma properties were used. This method is supported by the spatial separation of the Y-parameter values for decomposed Alfvénic (A-mode) and compressible (C-mode) MHD modes, which respectively decrease and increase with the inclination angle between the mean magnetic field and the line of sight, θ_λ. A statistical demarcation at $\mathrm{Y_{turb}} \sim 1.5$ (with $\mathrm{Y_{turb}} > 1.5$ for A-mode and $\mathrm{Y_{turb}} < 1.5$ for C-mode) is used to identify the dominant MHD turbulence mode in a given region. Moreover, the unique sensitivity of the $\mathrm{Y_{turb}}$ parameter to θ_λ in different MHD mode–dominated regimes (see Fig. 4 in Malik et al. 2023) enables estimation of θ_λ for certain morphologies. The method has been further applied and validated in subsequent studies using the Effelsberg polarisation observations of the extended Monogem pulsar wind nebula and the Cygnus-loop SNR (Malik et al., 2024; Malik and Pavaskar, 2026), demonstrating its robustness. However, the original technique (Malik et al., 2023) was developed under conditions of very weak Faraday rotation.

The arcsecond angular resolution of SKA AA4 at a Galactic Centre distance of ~ 8.5 kpc can resolve scales of about ~ 0.04 pc, well suited to the required high physical resolution (sub-pc to a few tens of pc) in this approach of the Y-parameter method. Furthermore, the compressible MHD turbulence mode has been identified as a major contributor to particle acceleration and scattering, leading to high-energy emissions in the GeV and TeV range, particularly the extended emission from pulsar wind nebulae and supernova remnants up to 50 pc in extent (Abeysekara et al., 2017; Liu et al., 2019). With SKA's resolution and sensitivity, MHD turbulence within the Galactic plane, including the Galactic Centre, can be mapped extensively, which is crucial for understanding cosmic-ray scattering and acceleration in detail.

2.1.3 Faraday Rotation – Rotation Measure

As linearly polarised emission propagates through a medium of ionised plasma with magnetic fields along the propagation direction, the emission experiences the Faraday rotation effect that leads to a rotation of the polarisation plane. Through multi-wavelength polarisation measurements, the Faraday rotation effect can be quantified by a parameter called the rotation measure (RM):

$$\Psi(\lambda^2) = \Psi(0) + 0.81 \int_L^0 n_e(s) B_\parallel(s)\, \mathrm{d}s \cdot \lambda^2 \equiv \Psi(0) + \mathrm{RM} \cdot \lambda^2, \tag{1}$$

where Ψ [rad] is the linear polarisation position angle at the electromagnetic-wavelength-squared λ^2 [m^2], L [pc] is the physical distance from the observer to the synchrotron-emitting source along the line-of-sight s, n_e [cm^{-3}] is the thermal electron number density, and $B_\parallel$ [μG] is the magnetic field component along s (e.g. see Ferrière et al., 2021). In galactic magnetism studies, RM is often obtained through radio observations of synchrotron-emitting sources such as galactic diffuse emission (e.g. Van Eck et al., 2017), pulsars (e.g. Sobey et al., 2021), active galactic nuclei (AGN) and radio

galaxies (e.g. Ma et al., 2020), and fast radio bursts (FRBs; e.g. Pandhi et al., 2024). Subsequently, the magnetic field strength, scale, and structure in the intervening medium can be retrieved from the RM values, given ancillary information about the spatial distribution of the thermal electrons.

With a dense sampling of background source RM across the sky, one can form a so-called RM-grid (Gaensler et al., 2004) that reveals the average magnetic fields in the intervening volume across spatial scales. The minimum scales probed are limited by the source density of the RM-grid. Given the presence of small-scale magnetic structures in the intervening galactic volume ($b_{\rm iso}$ and $b_{\rm ani}$), the RM values can be found to correspondingly exhibit spatial variations. Thus, the scale of magnetic fields in galaxies can be quantitatively studied by careful consideration of the spatial RM fluctuations. Specifically, the source-pair RM structure function (SF) analysis, as depicted in Figure 1 left column, is frequently utilised to statistically measure the spatial RM variations (e.g., Minter and Spangler, 1996; Stil et al., 2011; Seta and Federrath, 2024). With a polarised source density of $\approx 100\,{\rm deg}^{-2}$ that we can expect from SKA AA4 surveys, source-pair RM SF studies will be sensitive to magnetic structures from $\gg$ deg to $\approx$ arcmin scales (the corresponding physical scale in the system will depend on the distance).

Alternatively, RM fluctuations can be revealed by the RM maps of spatially resolved polarised emission (e.g. Haverkorn et al., 2004; Mao et al., 2015). In principle, the (per-source) RM SF analysis (see Figure 1 middle column) can be applied to RM maps of background AGN and radio galaxies to reveal galactic magnetic structures at scales between those of the radio sources (up to $\approx 10\,{\rm arcmin}$) and the angular resolution of the observations ($\approx$ arcsec with the SKA AA4). However, this has not yet been attempted, as such studies require the combination of (1) high angular resolution ($\ll$ arcmin), (2) high sensitivity (translating to per-beam RM uncertainty of $\ll 10\,{\rm rad\,m}^{-2}$), (3) moderate sky-area coverage ($\gg$ deg^2; to gather a statistically meaningful sample), and (4) a sufficient control sample that do not experience spatial RM variations due to foreground galaxies (see below). This has just been enabled recently by the exquisite polarimetric data from the many ongoing surveys conducted with SKA precursor telescopes, such as MMGPS (Padmanabh et al., 2023) with MeerKAT and SPICE-RACS (Thomson et al., 2023, in press) and POSSUM (Gaensler et al., 2025) with ASKAP, and will certainly warrant focus over the coming years in preparation for the SKA (see Sec. 5.1). Specifically, the exact details of the method will need to be fine-tuned using the SKA precursor survey data. Firstly, it is known that the magneto-ionic medium within/surrounding the background sources can contribute to the observed spatial RM variations (e.g. Ma et al., 2019; Baidoo et al., 2023). This component of RM fluctuations will therefore need to be carefully removed in a statistical manner (see Sec. 5.1), using information from a representative control sample (as mentioned above), to yield the galactic RM fluctuations that we are after. In addition, the RM SF from a single source is expected to be subjected to the stochastic nature of small-scale magnetic structures and therefore *not* representative to the overall characteristics of $b_{\rm iso}$ or $b_{\rm ani}$. Hence, the per-source RM SF from a moderate number of sources that are closely separated in the sky will need to be combined in some ways to unveil the underlying statistical properties of the galactic small-scale magnetic fields.

Another challenge in the analysis of RM SF arises from the numerical methodology. Standard two-point calculation may not provide accurate results, particularly when small-scale fluctuations have a

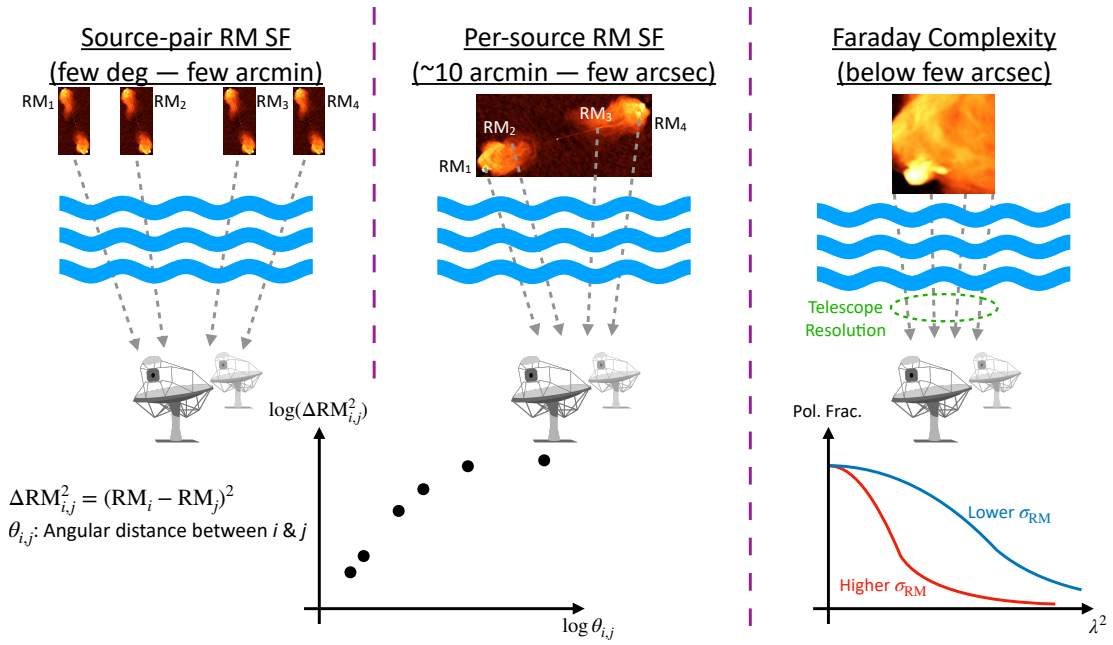

Figure 1: Schematics illustrating the Faraday rotation analysis methods, namely rotation measure structure function (RM SF; Sec. 2.1.3) and Faraday complexity (Sec. 2.1.4), that can be deployed with the SKA for small-scale galactic magnetic field studies. The corresponding angular scale range that each method is sensitive to is included in the title. The blue wave patterns represent the intervening galactic ISM. The formula in the figure presents RM SF computation with two points and this could also be generalised to n-points, which enables testing convergence in statistical properties of the small-scale magnetic fields from observations (Seta et al., 2023; Seta and Federrath, 2024). Image credits: the Australian Academy of Science (SKA-Mid dishes clip-art); NRAO/AUI (Cygnus A radio image).

larger power spectral slope and higher-order stencils involving more than two points can be required (see Sec. 2 in Seta et al., 2023). Such multi-point calculations also improve the separation of large- and small-scale magnetic field components (Seta and Federrath, 2024) and could also potentially help remove the contribution from the large-scale field structures and gradients. In addition, they enable convergence tests by verifying whether the inferred statistical properties of magnetic fields remain stable as the number of points in the computation increases (Seta et al., 2023).

2.1.4 Faraday Rotation – Wavelength-dependent Depolarisation (Faraday Complexity)

As discussed above in Sec. 2.1.3, the galactic small-scale magnetic fields can lead to spatial variations of the observed RM. For cases where there are significant RM variations at angular scales smaller than that of the background sources or the angular resolution (whichever is smaller), the polarised emission from the background source through different lines-of-sight within the telescope beam can individually experience a random walk in Faraday rotation (Burn, 1966; Sokoloff et al., 1998). Because of this, even if the polarisation planes of the emission are originally aligned among the different lines-of-sight, the eventual emission reaching the telescope can have misaligned polarisation planes due to the differing amount of Faraday rotation[3]. This leads to the observed

[3]This can also be regarded as a mix of linearly polarised emission experiencing different RM within the beam volume.

wavelength-dependent depolarisation effect, also commonly called Faraday complexity or Faraday depolarisation. By considering the observed linear polarisation signal across a broad frequency range using techniques such as RM-Synthesis (Brentjens and de Bruyn, 2005) and Stokes QU-fitting (Farnsworth et al., 2011; O'Sullivan et al., 2012), one can infer the magnitude of RM variations at spatial scales smaller than the telescope beam (see Figure 1 right column), enabling the statistical study of the intricate small-scale magnetic fields in the foreground volume.

Thus far, the technique of wavelength-dependent depolarisation has been applied to the study of the small-scale magnetic fields in the Milky Way (via background sources: Livingston et al., 2021; Ranchod et al., 2024; Ma et al., 2025, and via the Galactic diffuse emission: Van Eck et al. 2019; Erceg et al. 2022), as well as external galaxies near (via diffuse emission of the target galaxies; Gaensler et al., 2005; Mao et al., 2015; Basu et al., 2017) and far (via background sources; Mao et al., 2017; Kovacs et al., 2026). The key advancements that the SKA AA4 will bring are the broad instantaneous frequency coverage[4], surface brightness sensitivity, and angular resolution. All these combined will enable accurate studies of magnetic structures that are at least an order of magnitude smaller than is feasible with current-generation instruments. While the $\approx$ arcsec angular resolution of SKA AA4 will already set useful upper limits in the physical scale of the magnetic structures probed through Faraday complexity, we point out the advantages of stringent angular scale measurements (in the $\ll$ arcsec regime) that can be made available by other radio studies. These include (but are not limited to) direct measurements from (wide-field) Very Long Baseline Interferometry (VLBI), as well as indirect inferences from interplanetary scintillation (IPS) studies (Morgan et al., 2018). Similar to the case of per-source RM SF studies (above in Sec. 2.1.3), a precise probe of the galactic small-scale magnetic fields through Faraday complexity analysis will first require adequate knowledge of the intrinsic properties of the Faraday complexity exhibited by the background sources themselves (Ma et al., 2025).

Finally, we highlight the prospects of the extreme case of wavelength-dependent depolarisation, where many of the intrinsically polarised sources are completely depolarised. This has already been illustrated with the ASKAP POSSUM survey (Gaensler et al., 2025) for the case of the Galactic mid-plane (Vanderwoude et al., 2024) and for the Small Magellanic Cloud (SMC; Price et al., *submitted*). In particular, the effect of Faraday depolarisation can be deduced from the decrease in the polarised source density. Such analysis method will require (1) sensitive observations (yielding a polarised source density of $\gg 10\,\mathrm{deg}^{-2}$ without depolarisation), (2) moderate sky-area coverage ($\gg 10\,\mathrm{deg}^2$), and (3) excellent knowledge of the polarised source population. All three are expected to improve with SKA.

2.1.5 Zeeman Effect

As summarised in a concurrent SKA Science Chapter (see Robishaw et al., 2026), spectral line measurements of the Zeeman effect (in particular for HI and OH; both covered by the SKA-Mid Band 2) will be a powerful, direct *in-situ* tracer of the line-of-sight component of magnetic fields in the Milky Way and nearby galaxies. The HI Zeeman effect can be realistically detected in both the diffuse emission and absorption towards bright background sources, while that in OH can be

[4] With a broad coverage in λ^2, one can characterise Faraday complexity with higher accuracy with RM-Synthesis and Stokes QU-fitting (e.g. Brentjens and de Bruyn, 2005; Anderson et al., 2016; Kovacs et al., 2026; Van Eck et al., 2026).

performed towards (mega-)masers. We reiterate the comment from both the previous (Robishaw et al., 2015) and the contemporary (Robishaw et al., 2026) SKA Science Chapters that high precision wide-field correction in the instrumental circular polarisation will be pivotal to the success of future Zeeman experiments with the SKA-Mid.

2.2 Special Considerations

Observational probes of the small-scale magnetic field are different for the Milky Way and for other nearby galaxies. One of the most obvious differences is the physical scales concerned when using the diffuse synchrotron emission – greater than a few 100s of pc for most nearby galaxy studies (e.g. Kierdorf et al., 2020), while in the Milky Way, we can be sensitive to $\lesssim$ pc scales. Another key difference between the Milky Way and other galaxies is the line-of-sight depth of the field compared with the distance, applicable to both diffuse emission and RM-grid studies. Adjacent lines of sight are located on a cone with an opening angle equal to the angular distance between sky positions. For nearby galaxies, even in the Local Group, the intersection of that cone with the object is, to a good approximation, cylindrical, while for the Milky Way, the intersection is almost always a cone that probes smaller scales in the local ISM and larger scales in the more distant ISM.

2.2.1 Milky Way

The most significant probe of small-scale structure in the magnetic fields of the Milky Way by the SKA will be through Faraday rotation of a very large number of extragalactic sources (Sec. 2.1.3), supplemented by that from a large number of pulsars with reliable distance estimates (e.g. Sobey et al., 2019). The SKA will provide a giant step forward through a combination of factors. The smallest scale structures that can be probed by an RM-grid depend critically on the polarised source density. This is because of both the direct need for a fine spatial sample, and also because averaging across multiple sources is required to remove the stochastic nature of ISM turbulence (and the intrinsic RM contributions). With the large number of pulsars expected to be discovered with the SKA (e.g. $\approx$ 9,400 with the SKA-Low; Xue et al., 2017), their RM and dispersion measure (DM) combined, in addition to parallax distances, will allow for a detailed 3D probe of magnetic fields and thermal electron density in spiral arms and interarm regions (see Han, 2017; Curtin et al., 2024; Dhakal and Seta, 2025, and references therein).

2.2.2 Nearby galaxies

Thus far, the study of the magnetic fields in external galaxies via RM-grids is only feasible for the Magellanic Clouds (Gaensler et al., 2005; Livingston et al., 2022, 2024, Price et al. *submitted*, and references therein), M 31 (Han et al., 1998, as well as the Local Group L-Band Survey: Kovacs et al. *in prep.*), and a handful of lensing galaxy systems (Mao et al., 2017; Kovacs et al., 2026). The SKA will improve significantly on this, with the potential to reveal the small-scale magnetic field in the outer halo of many Local Group galaxies.

The energy injection scale in the interstellar medium, roughly 100 pc, corresponds to $4''$ at a distance of 5 Mpc. For galaxies outside the Local Group, they can impose significant wavelength-dependent (Faraday) depolarisation to the background polarised sources (Sec. 2.1.4). High angular resolution is key to improving the contrast between the background source and the emission of the foreground

galaxy. Probes of halo and/or circumgalactic medium magnetic fields in nearby galaxies are still possible, as demonstrated by the statistical analysis of Heesen et al. (2023).

2.3 Connecting SKA Observation with Numerical Simulations

To fully harness the diagnostic power of broadband polarimetry, parallel theoretical efforts are advancing. Recent developments (in covariant polarised radiative transfer formalism; Chan et al., 2019; On et al., 2019, see also Chapter of Chan et al. 2026) have unlocked the possibility of direct interfacing with galactic or cosmological magneto-hydrodynamics (MHD) simulations to produce accurate predictions of the polarised sky. This forward-modelling framework can treat point sources and diffuse magnetised media either together or separately, and computes the full Stokes spectra and high-fidelity polarisation and RM maps, enabling realistic synthesis of the complex Faraday behaviour observed in cosmic media. Naturally, this can allow production of mock SKA observations from numerical simulation results. This integration of forward modelling, measurement modelling, and inverse inference establishes a self-consistent framework for decoding Faraday complexity, allowing emission and propagation effects to be disentangled within the magneto-ionic interstellar medium. By closely integrating both observations and simulations, this approach provides a reliable platform for discovery, and predictive exploration of magnetic field evolution and Faraday complexity across galactic environments and beyond, fully leveraging the capabilities of SKA.

3 Scientific Goals

To understand the physics of the small-scale turbulent dynamo and the role of small-scale magnetic fields on a range of scales, especially in star formation and galaxy evolution (Sec. 4), it is essential to examine their strength, scale, and structure within galaxies. In this Section, we summarise the current state of knowledge and highlight the open questions in each of these areas.

3.1 Strength

From depolarisation observations and Faraday rotation measurements, it is estimated that the small-scale magnetic fields in the Milky Way and nearby galaxies are of the order of $5 - 20\,\mu$G (Gaensler et al., 2005; Mao et al., 2008; Haverkorn, 2015; Beck, 2016; Beck et al., 2019; Livingston et al., 2022; Seta et al., 2023; Livingston et al., 2024). The small-scale field strength is often comparable to, or even greater than, that of the large-scale field. Such a dynamically strong field can influence local gas flows (Planck Collaboration et al., 2016) and provide additional pressure that inhibits the collapse of gas into stars, thereby reducing the star formation efficiency. A key open question is what fraction of this field strength arises from amplification by the small-scale dynamo and what fraction results from the tangling of the large-scale field. Addressing this will constrain the physics of the small-scale dynamo and provide insights into the strength and properties of the turbulence responsible for tangling the large-scale field.

Another important prediction from small-scale turbulent dynamo theory and numerical simulations concerns the ratio of magnetic ($E_{\rm mag}$) to turbulent kinetic ($E_{\rm kin}$) energy densities and its dependence on the ISM phase ($E_{\rm mag}/E_{\rm kin} \approx 0.1$ in the warm/hot phase and ≈ 0.01 in the cold phase is inferred from numerical simulations, see Seta and Federrath, 2022; Gent et al., 2023). These numerical experiments, and the associated estimates of the $E_{\rm mag}/E_{\rm kin}$ ratio, primarily refer to small-scale

magnetic fields amplified by the small-scale turbulent dynamo and may change when additional processes, such as the large-scale dynamo and the tangling of large-scale magnetic fields, are included. Observationally, based on pulsar and Zeeman measurements, it has recently been shown that the magnetic energy density scales with the turbulent kinetic energy (Seta and McClure-Griffiths, 2025), although the precise fraction, $E_{\rm mag}/E_{\rm kin}$, as a function of ISM phase (and possibly also on the galactocentric radius, as shown for the total field in Beck, 2007, 2015), remains difficult to determine. Constraining this ratio would provide a direct measure of the efficiency of the small- and large-scale dynamo in different phases and strengthen our understanding of the ISM–magnetic field connection.

3.2 Scale

The correlation scale of the small-scale ISM magnetic fields in the synchrotron-emitting and Faraday-rotating plasma is primarily estimated using two methods: RM structure functions and depolarisation models. For the Milky Way, this scale lies in the broad range 1–100 pc depending on location in the Galactic disk (Haverkorn et al., 2008), although recently estimated to be within 20–30 pc using pulsars for the volume-filling, ionised ISM (Dhakal and Seta, 2025). For nearby irregular galaxies, it is larger, with values of $\approx$ 160 pc for the Small Magellanic Cloud and $\approx$ 90 pc for the Large Magellanic Cloud (Gaensler et al., 2005; Seta et al., 2023). For grand-design spiral galaxies, this has been estimated to be about 50 pc (Fletcher et al., 2011). In contrast to field strength, where the physics of converting turbulent kinetic energy into magnetic energy and the associated local magnetic field compression is relatively well understood, the description of magnetic field scales in terms of ISM properties remains missing. Establishing a predictive relationship between magnetic field scale and ISM properties would clarify the role of the ISM in shaping these scales and provide stronger constraints on cosmic-ray propagation (e.g. see Sec. 4.1).

The smallest magnetic field scales observable in the ISM must naturally be positioned close to the Sun. One of the nearby highly magnetised structures predominantly lies along the walls of the Local Bubble (Alves et al., 2018; O'Neill et al., 2025). These regions are shaped by recent star formation activity and the cumulative effects of stellar winds and supernova explosions, which have carved out and compressed the surrounding medium. Prominent examples include H II regions such as Sh2-27 (Raycheva et al., 2022), star-forming molecular clouds like the Orion complex, and various supernova remnants that trace small-scale, turbulent magnetic fields on sub-parsec scales.

All theories of MHD turbulence and the small-scale dynamo predict a power-law magnetic field power spectrum (Schekochihin, 2022), with a slope that depends on the specific theory. Reliably determining this slope from radio observations, potentially using multi-point RM structure functions with higher-order stencils (Seta et al., 2023; Seta and Federrath, 2024), would provide further insight into the plasma physics of the ISM.

3.3 Structure

Based on MHD turbulence and small-scale dynamo theories, the small-scale magnetic fields in galaxies are expected to be random but non-Gaussian, with strong fields concentrated in filamentary or sheet-like structures (Zel'dovich et al., 1987; Subramanian, 1998; Schekochihin et al., 2002). This behaviour is seen in a variety of simulations (Schekochihin et al., 2004; Haugen et al., 2004;

Seta et al., 2020; Seta and Federrath, 2021; Basu and Sur, 2021; Sur and Subramanian, 2024), and some ISM observations also reveal filamentary structures (e.g., Zaroubi et al., 2015; Erceg et al., 2022; Heywood et al., 2022; Yusef-Zadeh et al., 2022). However, the lack of finely spaced data has so far prevented a detailed observational study of magnetic field structure. Characterising the morphology of these structures using topological methods (e.g., Minkowski functions, Betti numbers, and persistence diagrams, see Wilkin et al., 2007; Makarenko et al., 2018a,b; Seta et al., 2020; Dwivedi et al., 2024; Dutta et al., 2024) would not only constrain theoretical parameters but also allow us to better quantify the local impact of magnetic fields on gas flows and star formation.

Moreover, a precise understanding of the structure of the magneto-ionic medium of the Milky Way, even in a statistical sense, is crucial for effective foreground determination, particularly in the context of Faraday rotation. Across angular scales ranging from degrees (comparable to the apparent size of nearby galaxy clusters) down to the effective point-source level, Galactic structures can easily be mistaken for larger-scale RMs (such as from galaxy groups or clusters, see Anderson et al., 2024, for a discussion), and vice versa. Furthermore, the anisotropy of the magnetic field structure, which may be linked to gaseous motions in the ISM, ought to be further understood and its origins clarified.

For studies of extragalactic structures, this issue is commonly mitigated by focusing on high Galactic latitudes and employing large-scale models to subtract the Milky Way contribution. Conversely, the inference of the Galactic RM has traditionally relied on the assumption that extragalactic RMs are uncorrelated and point-like in nature (Hutschenreuter et al., 2022). However, at the angular resolutions achievable with SKA (both Low and Mid), and given our current understanding of Milky Way structure, neither assumption is likely to remain valid to the required precision. Thus, robust methods for characterising magnetic structures both in the source and foreground and their standardisation with MHD simulations are necessary to fully exploit the upcoming SKA data.

The quality of foreground removal depends sensitively on both the source density and analysis methods employed (e.g. the interpolation kernel, as discussed in Khadir et al., 2024). Notably, the structure-function analysis, discussed in Sec. 2.1.3, is also directly connected to the underlying correlation function of foreground structures, which in turn determines the interpolation kernel for this purpose.

4 Highlights of Specific Scientific Questions

In this Section, we highlight a few key outstanding scientific questions in the field of small-scale magnetic fields in galaxies. Then in Sec. 5.3, we will describe how future SKA observations will significantly advance our understanding in these areas.

4.1 Magnetic Fields in Molecular Clouds and *in-situ* Synchrotron Emission

One of the most powerful probes of magnetic fields in the ISM is synchrotron emission (see Sec. 2.1.1). However, no detectable synchrotron emission has been observed from the molecular cloud cores (see recent work regarding possible synchrotron emission from the boundary of molecular gas in Bracco et al., 2023), even though Zeeman effect observations show strong magnetic fields ($\gtrsim 10\,\mu$G, e.g., Crutcher et al., 2010). This raises further questions about the strength and geometry of mag-

netic fields, the sites of star formation, and the propagation of low-energy cosmic ray electrons in molecular clouds.

The most recent data from the *Voyager* probes (Cummings et al., 2016; Stone et al., 2019), together with detections provided by the *Fermi Large Area Telescope* (*Fermi-LAT*; Ackermann et al. 2010), the balloon-borne Pamela experiment (Adriani et al., 2011), and the Alpha Magnetic Spectrometer (AMS-02) on board the International Space Station (Aguilar et al., 2014), constrain the local cosmic-ray electron flux down to energies relevant for synchrotron emission.

The average magnetic field strength in molecular clouds could be weaker than that shown by Zeeman measurements, which primarily trace the dense regions. Ambipolar diffusion might be the reason for the average weaker fields (Tritsis, 2025). A more significant issue, however, is the penetration of low-energy (primarily GeV) cosmic ray electrons (Dickinson et al., 2015). The ISM is filled with low-energy cosmic ray electrons, and magnetic field lines connecting the relatively warm ISM around the molecular clouds to the cold gas within the molecular clouds should allow them to enter. There are, however, two related issues. First, cosmic ray electrons lose energy rapidly, with the loss rate proportional to the square of the magnetic field strength, which remains poorly constrained in and around molecular clouds. Second, the magnetic field structure at cloud boundaries may create particle traps (Cesarsky and Volk, 1978; Chandran, 2000; Seta et al., 2018; Silsbee et al., 2018), further enhancing energy losses through increased confinement times. Both effects limit cosmic ray electron penetration. In that case, synchrotron emission would originate mainly from the boundary or outer regions of molecular clouds, but probably at levels too low to be detected with current facilities (Wolleben and Reich, 2004; Bracco et al., 2025). With the superior sensitivity of the SKA-Low, *in-situ* synchrotron emission from molecular clouds, likely from their envelopes, will likely become detectable (Sec. 5.3.1). Such observations will constrain the strength and geometry of magnetic fields in and around molecular clouds and shed light on the propagation of cosmic ray electrons.

Understanding how cosmic rays propagate through the ISM and dense clouds offers valuable insight into their distribution, and therefore, their coupling with the gas and potential feedback effects. If free-streaming penetration of electrons in molecular clouds holds (Takayanagi, 1973; Padovani et al., 2009), the relativistic part of the cosmic-ray electron spectrum turns out to be unaffected during the propagation up to H_2 column densities of approximately 10^{23} cm^{-2}, which are characteristic of the densest regions of molecular clouds (Padovani et al., 2018). In this case, Padovani and Galli (2018) showed that for typical expected magnetic field strength in starless cores ($< 10^3$ μG), the detection of synchrotron radiation depends on the integrated line-of-sight value of the magnetic field strength, which, in turn, is determined by the density profile. As a consequence, synchrotron flux should be larger for a dense core with a shallow density profile compared to a core with a peaked density profile. For example, SKA should detect synchrotron emission at frequencies of $\sim$ 200 MHz reaching a signal-to-noise up to $\sim$ 7 and $\sim$ 2 in one hour of integration for starless cores such as FeSt 1-457 in the Pipe Nebula and Barnard 68, respectively. Low-frequency SKA observations, combined with other innovative methods for estimating magnetic field strength, will therefore provide useful information on the propagation of cosmic rays in molecular clouds, clarifying whether free-streaming is a good approximation for cosmic-ray transport. If not, it would imply that cosmic-ray

motion is slowed down by scattering off magnetic field fluctuations on scales comparable to their gyroradius.

One final important aspect to consider is that the description of synchrotron emission is usually made assuming a single energy slope for the CR electron spectrum. However, *Voyager* data indicate that the local Galactic cosmic-ray electron spectrum bends at low energies. If this is the case, the standard frequency-magnetic field-energy relation (see e.g. Longair, 2011) does not hold anymore and there is no unique correspondence between energy slope and spectral index slope. Thanks to SKA's high frequency resolution, it will be possible to compare independent estimates of the spectral index obtained over a series of narrow frequency intervals, and then trace back the variation in the energy slope of the cosmic-ray electron spectrum (Padovani et al., 2021; Linzer et al., 2025).

4.2 The Interplay between Small-scale Magnetic Fields and Star Formation Processes

It has been well established that turbulence and magnetic fields can regulate the star formation rate and influence the stellar initial mass function (Federrath and Klessen, 2012; Krumholz and Federrath, 2019; Mathew et al., 2023; Pattle et al., 2023). While the effects of the molecular cloud magnetic fields have been explored observationally (via dust and starlight polarisation studies; Planck Collaboration et al., 2016; Li et al., 2017), the roles of the magnetic fields throughout the baryon cycle, especially the cooling and condensation of the warm/hot ISM phases to the cold gas phases, remain poorly understood. Although measurements of the magnetic field strength across ISM phases exist (e.g. Crutcher et al., 2010; Harvey-Smith et al., 2011; Thomson et al., 2018; Seta and McClure-Griffiths, 2025), it is crucial to obtain observationally derived information on the magnetic field strength, scale, and structure *combined* across all ISM phases (Sec. 3). This will be the key to understanding how magnetic fields co-evolve with galaxies, addressing one of the central questions in modern astrophysics. This is particularly the case for the small-scale ($b_{\rm iso}$ and $b_{\rm ani}$) components of the magnetic fields (Sec. 1), given the relevance in spatial domain (at $\lesssim 100\,$pc), as well as their dominance in strength over the large-scale coherent magnetic field (Beck, 2016).

Further, the exact astrophysical origin of the radio-infrared correlation in star-forming galaxies remain obscured (see Beck and Wielebinski, 2013; Beck, 2016). While it is understood that both emission are linked to star-formation activities, the details for the radio (synchrotron) emission are unclear. Specifically, the total (dominated by $b_{\rm iso}$ and $b_{\rm ani}$) magnetic field strength, which is responsible for the observed synchrotron intensity, can either be amplified by shocks in star-formation feedback processes, or by compression (due to gravity) during the stage of cloud collapse. This can be answered by future high angular resolution, high sensitivity observations of Galactic and extragalactic star-forming regions.

While we anticipate that the on-going SKA precursor polarisation surveys (Padmanabh et al., 2023; Gaensler et al., 2025) can begin to address the above in the coming few years, it will almost certainly lead to discoveries that warrant follow-up studies. Compared to the SKA precursor telescopes, the SKA will offer greatly enhanced sensitivity and angular resolution, allow us to explore the galactic magnetic fields at much smaller spatial scales and at much higher accuracy than is currently feasible (Sec. 5.2).

4.3 Magnetic Fields in Elliptical Galaxies

Most studies of magnetic fields focus on star-forming galaxies (Beck, 2016), but it is also important to examine magnetic fields in ellipticals that, at most, are forming stars near their centres at low rates. Since ellipticals lack significant differential rotation, the conventional α-Ω large-scale dynamo does not operate, and the small-scale field produced by the tangling of a large-scale field is negligible. This makes ellipticals a more pristine environment for probing the properties of small-scale dynamo (Moss and Shukurov, 1996; Seta et al., 2021).

Using the Laing-Garrington effect (Laing, 1988; Garrington et al., 1988) for ellipticals with an active host and a statistical study of intervening elliptical galaxies, it is inferred that the typical magnetic fields in ellipticals ($\lesssim 1\,\mu$G) are about an order of magnitude weaker than those in star-forming disk galaxies (Seta et al., 2021; Shah and Seta, 2021). Alternative methods are hindered by various limitations, such as the detection of the diffuse synchrotron emission from the elliptical galaxies can be contaminated by the central sources (namely, AGN) and can be challenging given the sparse cosmic ray electrons, while the use of physically unrelated background source RM is limited by the insufficient RM-grid density. The expected synchrotron emission from the ISM of ellipticals at ≈ 100 MHz is only ≈ 25 nJy (see Sec. 5.3 in Seta et al., 2021), which will remain challenging for a direct detection even with SKA. Thus, the most effective probe of magnetic fields in ellipticals will be the high RM source density expected with SKA (Sec. 5.3.3).

4.4 Magnetic Fields in Intermediate-redshift Galaxies

To constrain the parameters of the dynamo theories (both small-scale, fluctuation dynamo and large-scale, α-Ω dynamo), it is important to observe magnetic fields in galaxies across cosmic time. This can be done by measuring the magnetic field growth rate and scale as a function of redshift. Recent efforts studying gravitationally lensing galaxies (Mao et al., 2017; Kovacs et al., 2026) have captured both the large- and small-scale magnetic fields in the foreground lensing galaxies, highlighting the prospects of the innovative technique. We refer the readers to the Mao et al. (2026) Chapter for discussions on the large-scale magnetic fields and focus on the small-scale magnetic fields here (see also Sec. 5.3.4). With the SKA, we shall greatly expand the number of sampled lensing galaxy systems, and thereby explore the properties of the small-scale galactic magnetic fields across redshift and various galactic parameters (e.g. star formation rate and stellar mass).

5 Preparation for and Plans with the SKA

5.1 Preparation with SKA Precursors

From early-mid 2020s, high quality polarimetric data from SKA precursor surveys, such as MMGPS with MeerKAT (Padmanabh et al., 2023), POSSUM with ASKAP (Gaensler et al., 2025), and LoTSS with LOFAR (O'Sullivan et al., 2023), have been made available in abundance. These data will be crucial in the lead up to the SKA AA* and AA4 for the study of small-scale magnetic fields in galaxies, as well as cosmic magnetism in general, as we describe in more details below.

The anticipated advent of the SKA will bring a multitude of advancements in the context of the study of the galactic small-scale magnetic fields with respect to the current state-of-the-art (Sec. 2

and 5.2). However, the SKA's full potential can only be realised given adequate preparations in both analysis algorithm development and our astrophysical knowledge in galactic magnetism. While the source-pair RM SF analysis is already sufficiently mature (e.g. Seta et al., 2023), the per-source RM SF method (Sec. 2.1.3) that will allow us to explore the sub-arcmin regime will still require significant progress. This includes both the removal of the RM SF contributions by the emitting AGN and radio galaxies, and the specifics of averaging across multiple sources to uncover the underlying statistical signal. Similarly, the Faraday complexity (wavelength-dependent depolarisation) technique (Sec. 2.1.4) will require further development in the coming years. While the general analysis framework has already been set by recent works (Livingston et al., 2021; Ranchod et al., 2024; Ma et al., 2025), the need for an accurate removal of the intrinsic Faraday complexity has been recognised.

Finally, as the study of small-scale galactic magnetic fields will likely see the most significant advancements from deep, small-sky-area SKA surveys rather than shallow, wide-area studies (Sec. 5.2), we ought to make use of the on-going wide-area SKA precursor surveys to identify (1) interesting Galactic regions, and (2) specific galaxy types (by, e.g., stellar mass, star formation rate, and redshift; also, see Chapter by Mao et al., 2026), for future SKA AA* and AA4 studies.

5.2 Considerations for SKA Observations

Here, we discuss the specific types of SKA observations that can benefit the study of small-scale galactic magnetic fields, in order to facilitate future commensal observations. The approximate linear polarisation performance of the SKA AA4 across different frequency bands is summarised in Table 1. Below in Sec. 5.3, we will outline potential large-scale SKA survey projects primarily driven by our particular science topic.

5.2.1 SKA-Low (50–350 MHz)

The most exciting aspect of SKA-Low will be the study of the local Galactic ISM through its diffuse polarised synchrotron emission (Van Eck et al., 2019; Erceg et al., 2022). The $\approx$ 9 arcsec ($\approx 4 \times 10^{-3}$ pc at 100 pc) resolution will reveal the highly intricate magnetic structures in the Solar neighbourhood and enable joint analysis with other tracers of the (magnetised) ISM such as dust polarisation (e.g. Planck Collaboration et al., 2016), starlight polarisation (e.g. Angarita et al., 2024; Panopoulou et al., 2025), and HI structures (e.g. Bracco et al., 2020; Ma et al., 2023).

Meanwhile, we expect that RM SF studies will see limited progress with the SKA-Low, given the scarce polarised source density (about 1–10 deg^{-2}; see Chapter by O'Sullivan et al., 2026)[5]. Although the SKA-Low will provide extremely precise RM values (measurement uncertainty $\lesssim 8 \times 10^{-3}\,\mathrm{rad\,m^{-2}}$), this key advantage will be less relevant for our case here given the RM uncertainty contributed by the intrinsic RM scatter of the extragalactic sources ($\approx 6\,\mathrm{rad\,m^{-2}}$; Schnitzeler, 2010). Though, we recognise that pulsars are believed to have minimal intrinsic RM (Wang et al., 2011) and Faraday complexity (Sobey et al., 2019). This makes the superior RM precision afforded

[5] This number is highly uncertain given our current limited knowledge in the polarised source population at such low radio frequencies. With LOFAR, the LoTSS RM catalogue DR2 (O'Sullivan et al., 2023) has achieved a polarised source density of 0.43 deg^{-2} at 144 MHz with a sensitivity of 83 μJy/beam; while a stacking study with the LoTSS data has provided 1.24 deg^{-2} with a sensitivity of 19 μJy/beam (Piras et al., 2024).

by the SKA-Low to be highly advantageous for pulsar RM studies, which in turn can provide significant insight into the small-scale Galactic magnetic fields (using and advancing the methods such as in Dhakal and Seta, 2025). For example, year/decade-long monitoring of pulsars with high proper motion can be used to trace the $\ll 0.01$ pc-scale magneto-ionic medium, given that the ionospheric RM is properly accounted for (Porayko et al., 2019).

Finally, we identify the prospects of SKA-Low Faraday depolarisation studies. With the high RM precision and low maximum Faraday depth extent ($\approx 4\,\mathrm{rad\,m^{-2}}$), SKA-Low observations of polarised extragalactic sources will be incredibly sensitive to the presence of weak small-scale magnetic fields that would otherwise be undetectable with higher frequency instruments (e.g. ASKAP, MeerKAT, & SKA-Mid). This is demonstrated in Figure 2, from which one can see that $\sigma_{\mathrm{RM}} \lesssim 1\,\mathrm{rad\,m^{-2}}$ can only be detected with high confidence the SKA-Low.

Overall, we consider a wide-area SKA-Low polarisation survey with a uniform sensitivity to be highly relevant to our science goal, provided that various undesirable effects such as ionospheric RM contributions and wide-field instrumental polarisation are carefully removed from the science-ready data.

5.2.2 SKA-Mid Bands 1 (350–1050 MHz) & 2 (950–1760 MHz)

These two frequency bands are likely the most relevant for the study of the small-scale galactic magnetic fields. We focus on the prospects of RM SF and Faraday complexity studies here, and refer the readers to Chapters by Sun et al. (2026) and Mao et al. (2026) for potential polarised diffuse emission works for the Milky Way and external galaxies, respectively. We further refer readers to Chapter by Robishaw et al. (2026) for details on direct magnetic field strength measurements with the Zeeman effect (noting that SKA-Mid Band 2 will cover both the HI and OH spectral lines).

Both of these frequency bands will provide excellent RM precisions ($\lesssim 0.4$ and $\lesssim 4\,\mathrm{rad\,m^{-2}}$ for Bands 1 and 2, respectively), sensitivity to Faraday complexity (with maximum Faraday depth extents of 38 and 108 $\mathrm{rad\,m^{-2}}$, respectively), and similar expected polarised source density (for a 1 hr observation, Bands 1 and 2 will likely yield 80–130 $\mathrm{deg^{-2}}$ and 100–130 $\mathrm{deg^{-2}}$, respectively). Given that Band 1 will be more sensitive to small RM fluctuations ($\sim 1\,\mathrm{rad\,m^{-2}}$; see Figure 2), it will be more suited for studies of sky regions with minimal RM fluctuations from the small-scale galactic magnetic fields (intermediate Galactic latitudes of beyond $\pm 10^\circ$ for the Milky Way; halos or circumgalactic medium for external galaxies). Meanwhile, Band 2 will be more robust against complete Faraday depolarisation (see Figure 3) and therefore will be the better choice for studies of sky areas with modest RM fluctuations ($\sim 10\,\mathrm{rad\,m^{-2}}$) such as the Galactic plane (within $\pm 10^\circ$ in latitude) as well as the galactic disks of nearby galaxies.

We further highlight the prospects of polarimetric studies of scintillating pulsars. Specifically, time-resolved measurements of Faraday rotation (both RM and Faraday complexity) can provide information on the small-scale magnetic fields on $\ll 1000$ AU scale. This will require the development of analysis methods analogous to the power spectrum of the pulsar dynamic spectrum (the "secondary spectrum"; e.g. Sprenger et al., 2022). We expect that observations with the SKA-Mid Bands 1 or 2 (or Band 3; for pulsars in extreme environments such as the Galactic Centre or along spiral arm tangents) will be the most useful.

5.2.3 SKA-Mid Bands 3 (1650–3050 MHz) & 4 (2800–5180 MHz)

These two SKA-Mid bands, which will be made available contingent on funding, are crucial for studying galactic areas with high levels of RM fluctuations ($\sim 50\,\mathrm{rad\,m^{-2}}$). This conclusion comes from their linear polarisation performance, with RM uncertainties of $\lesssim 12\,\mathrm{rad\,m^{-2}}$ (Band 3) and $\lesssim 35\,\mathrm{rad\,m^{-2}}$ (Band 4), as well as the maximum Faraday depth extents of $325\,\mathrm{rad\,m^{-2}}$ (Band 3) and $937\,\mathrm{rad\,m^{-2}}$ (Band 4). We note that, as at the time of writing, the exact sensitivities of the receivers remain unknown, but we assume that (similar to all other SKA-Mid frequency bands) a polarised source density of $\approx 100\,\mathrm{deg^{-2}}$ can be reasonably achieved with a 1 hr observation. As mentioned above, Bands 3 and 4 observations will be especially relevant for in-depth studies of extreme Galactic regions, such as the Galactic mid-plane (within $\pm 1^\circ$ in latitude), the Galactic Centre region, and ionised Galactic structures resulting from stellar feedback processes.

5.2.4 SKA-Mid Bands 5a (4600–8500 MHz) & 5b (8300–15400 MHz)

Finally, these two bands at the high end of the SKA spectrum can lead us to discover the unknowns — regions with extreme small-scale galactic magnetic fields that exhibit as small-scale RM fluctuations of $\gg 100\,\mathrm{rad\,m^{-2}}$ on $\lesssim$ arcmin scale. Such potential breakthroughs can be enabled by, for example, a Band 5a/5b Galactic plane survey in full polarisation.

5.2.5 SKA-Mid Survey for Small-scale Galactic Magnetic Fields — Wide or Deep?

Summarising the above information, and considering the performance of the on-going wide-area polarisation surveys with SKA-Mid precursors that will yield polarised source density of $\approx 30\,\mathrm{deg^{-2}}$ (Padmanabh et al., 2023; Gaensler et al., 2025), we believe that shallow ($\approx$ 1 hr per pointing), wide-area SKA-Mid surveys may not represent the generational leap that will be required to enable transformational discoveries in cosmic magnetism studies[6]. Therefore, we consider that deep, small-area SKA-Mid surveys will be the most promising for advancing our knowledge of the small-scale magnetic fields in galaxies. We point out that to bring an order-of-magnitude increase in the polarised source density with respect to the current-generation surveys (i.e. to $\gtrsim 300\,\mathrm{deg^{-2}}$), we will require SKA-Mid AA4 observations with per-pointing integration time (target sensitivity) of 20–80 hr (0.26–0.52 μJy/beam) for Band 1, 20–40 hr (0.18–0.26 μJy/beam) for Band 2, 60–140 hr (0.06–0.09 μJy/beam) for Band 5a, and 200–450 hr (0.04–0.06 μJy/beam) for Band 5b.

5.3 Potential Large-scale SKA Programmes

5.3.1 Magnetic Fields in Molecular Clouds

The detection of magnetic fields in diffuse molecular clouds across multiple radio tracers (namely, Zeeman effect, synchrotron emission, and Faraday rotation) *combined* will certainly shed light on magnetism's roles in ISM phase transitions and star formation (see also Tahani et al. 2026 Chapter). In particular, studies of nearby (distance ≈ 100 pc), off-plane ($|b| > 10^\circ$) systems in the southern sky such as the Chamaeleon and the Corona Australis will likely be the most fruitful. This is because of the combined advantages from (i) high resolution in physical scales, (ii) high background polarised

[6] One exception to this being a wide-area SKA-Mid Band 1 survey, as this frequency range can be highly potent for Faraday complexity studies (see above), yet poorly explored beyond the MMGPS-UHF survey. While the Band 5a/5b frequency range is similarly under-utilised, the low survey speed can make a wide-area survey prohibitive.

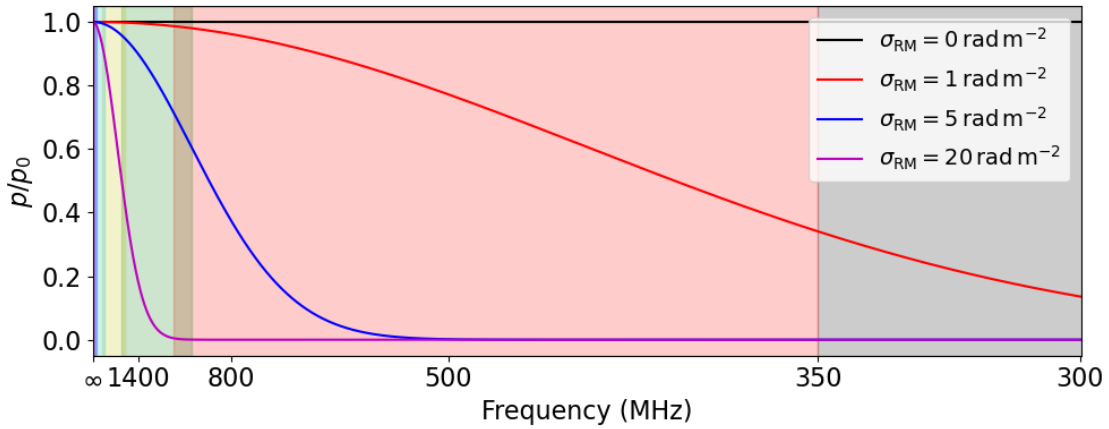

Figure 2: The effect of external Faraday dispersion (which exhibits $p \propto \exp(-2\sigma_{\rm RM}^2\lambda^4)$; Sokoloff et al., 1998) across the SKA frequency bands, with the solid coloured lines showing the results of different $\sigma_{\rm RM}$ values. The y-axis represents the ratio of observed-to-intrinsic polarisation fraction (1 for no depolarisation; 0 for complete depolarisation), and the x-axis is linear in λ^2 domain. The shaded areas represent (from right to left) SKA-Low (black; 50–350 MHz), SKA-Mid Band 1 (red; 350–1050 MHz), SKA-Mid Band 2 (green; 950–1760 MHz), SKA-Mid Band 3 (yellow; 1650–3050 MHz), SKA-Mid Band 4 (cyan; 2800–5180 MHz), and SKA-Mid Band 5a (blue; 4600–8500 MHz). SKA-Low is truncated at 300 MHz, and SKA-Mid 5b is omitted in this illustration.

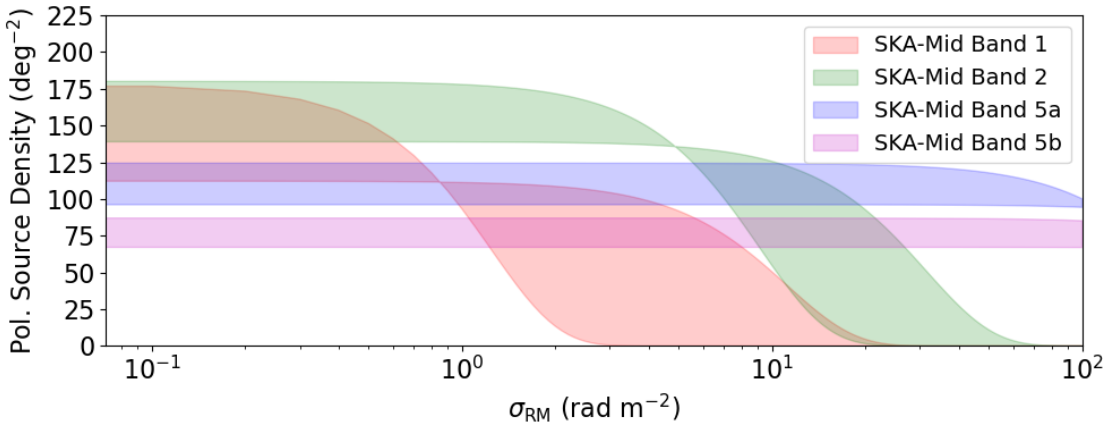

Figure 3: The number density of linearly polarised source that we expect to detect with a fiducial 1 hr SKA-Mid AA4 observation, as a function of the spatial RM fluctuation ($\sigma_{\rm RM}$). The depolarisation due to $\sigma_{\rm RM}$ follows $\exp(-2\sigma_{\rm RM}^2\lambda^4)$ (external Faraday dispersion; Sokoloff et al., 1998). For any given frequency band and $\sigma_{\rm RM}$ value, the span in y-value captures two frequency-dependent effects in the band – radio spectral index and Faraday depolarisation.

source count, (iii) minimal confusion with signals from the Galactic mid-plane, and (iv) availability of 3D density maps in the Solar neighbourhood (Edenhofer et al., 2024; Söding et al., 2025). The typical angular extent of such nearby molecular complexes is $\sim 10\,\mathrm{deg}^2$, meaning that deep observations ($\gtrsim 10$ hr per pointing) surveying their entirety are feasible with the SKA AA4. We note that synchrotron emission and Faraday rotation may not be sensitive to the magnetic fields in the densest

regions of molecular clouds[7] but nonetheless may be able to probe the intermediate/outer layers of such systems.

The aforementioned pursuit of the detailed characterisation of the magnetic fields in molecular clouds can be achieved with observations with the SKA-Low and the SKA-Mid in Bands 1 and 2. In particular, for the detection of synchrotron emission from molecular clouds, a 50 hr per-pointing SKA-Low survey will yield a sensitivity of 6.6 μJy per 4″ beam, which is a significant improvement over the current state-of-the-art (e.g. 83 μJy per 6″ beam with LoTSS; Shimwell et al., 2022). RM and Faraday complexity studies can be best performed with SKA-Mid Band 1, thanks to its high RM precision and sensitivity to Faraday depolarisation (Sec. 5.2). A 50 hr per-pointing Band 1 survey will deliver a sensitivity of 0.3 μJy per 1.3″ beam, corresponding to a polarised source density of 380–610 deg^{-2}, and thus leading to 3,800–6,100 RM and Faraday complexity measurements across the extent of each 10 deg^2 nearby molecular cloud. Finally, the SKA-Mid Band 2 covers both the HI and OH spectral lines, enabling direct measurements of the line-of-sight magnetic field strength and direction via the Zeeman effect. A concurrent recording of the Band 2 full-Stokes continuum data will further complement the Band 1 survey mentioned just above.

5.3.2 Interesting Galactic Regions; Magellanic Clouds; M 31

As described above in Sec. 5.1, the many on-going wide-area polarisation surveys with SKA precursor telescopes (e.g. Padmanabh et al., 2023; Gaensler et al., 2025) will almost certainly lead to discoveries regarding the small-scale magnetic fields in the Milky Way ISM, similar to the extreme |RM| towards the Sagittarius spiral arm tangent (Shanahan et al., 2019) recently unravelled by the Very Large Array (VLA) The HI/OH/Recombination line survey of the Milky Way (THOR; Beuther et al., 2016). The mysteries surrounding the new discoveries can be resolved with deep observations of the Milky Way and our cosmic neighbours (in particular, the Magellanic Clouds and M 31) with the SKA-Mid, leveraging on its exceptional sensitivity, high angular resolution, and broad instantaneous bandwidth combined.

The exact frequency band choice, as pointed out in Sec. 5.2, will depend on the properties of the sky area of interest. Specifically, regions subjected to severe Faraday depolarisation will require observations in the higher frequency bands (Band 2 or even Bands 3 and 4) at the cost of lower RM precisions; while regions exhibiting low levels of Faraday depolarisation will require observations in the low frequency range (Band 1) to detect the associated depolarisation effects, with the added benefit of higher RM accuracies. Meanwhile, the required per-pointing integration time will depend on the science requirements of the polarised source density (likely in the 100–1000 deg^{-2} range).

While we cannot predict the exact science directions that the SKA precursor surveys will steer us towards in the coming years, we list below a few potential Galactic areas that we may pursue with the SKA-Mid AA4:

- *Galactic Centre & Central Molecular Zone* — These are amongst the most extreme environments that can be found within the Milky Way (Eatough et al., 2013; Heywood et al., 2022; Paré et al., 2024), allowing us to explore the interplays between the ISM and Sgr A*, Galactic

[7] This is because of the expected low number density of cosmic rays (for synchrotron; because of shielding effects) and thermal electrons (for Faraday rotation; because of the low ionisation fraction).

outflows, and intense star formation. Moreover, the observed synchrotron filaments in the MeerKAT observations (Heywood et al., 2022; Yusef-Zadeh et al., 2022) suggest this region to be promising for studying the magnetic field structure (discussed in Sec. 3.3).

- *Galactic Anti-centre* — By looking away from the Galactic Centre region, one observes through a relatively calm sky area that is not saturated by stellar feedback processes (due to the shorter path-length and the lower star-formation rate), as well as less affected by the regular / anisotropic turbulent magnetic fields (since both are approximately perpendicular to the line-of-sight). Therefore, the Galactic Anti-centre can be an excellent target area for studying how individual star-forming regions can produce/sustain the isotropic turbulent magnetic fields.

- *Off-plane control regions* — We stress the importance of observing a control region away from the Galactic mid-plane that has minimal contributions by the Galactic small-scale magnetic fields. This is required to isolate the intrinsic Faraday complexity of the background extragalactic sources (Sec. 2.1.4 and 5.1). Given that the observed Faraday complexity can depend on the frequency coverage (Anderson et al., 2016) and signal-to-noise (O'Sullivan et al., 2017), information gathered from similar control experiments with the SKA precursors ought not be applied to future SKA studies. Instead, the control regions should be observed in an almost identical manner (i.e. frequency coverage and integration time) to the science observations.

- *Our closest neighbours* — Studies of the ISM of external galaxies are often more straightforward than those of the Milky Way, thanks to our external perspectives of the nearby galaxies. Amongst our cosmic neighbours, the Magellanic Clouds and M 31[8] can be SKA's prime targets for detailed studies of their small-scale magnetic fields, given their proximities to us ($\approx$ 50–65 kpc for the Magellanic Clouds; $\approx$ 770 kpc for M 31). With diffuse polarised emission, an assumed angular resolution of $5''$ translates to 1.2–1.6 pc for the Magellanic Clouds, and 22 pc for M 31 – sufficient for spatially resolving the $\ll$ 100 pc small-scale galactic magnetic structures. With background polarised sources, assuming a fiducial source density of $\approx$ 100 deg^{-2} (which will allow us to probe down to arcmin scales with source-pair RM SF analysis), we can explore down to physical scales of 15–19 pc for the Magellanic Clouds, and about 220 pc for the M 31.

5.3.3 Elliptical Galaxies

With the SKA AA4, we expect to be able to attain an in-depth knowledge of the magnetic fields in nearby elliptical galaxies and thus, how small-scale magnetic fields can be amplified and maintained in the absence of large-scale magnetic fields in galaxies (Sec. 4.3). With the background polarised sources as probes via Faraday rotation effects (by the enhanced RM scatter, and possibly by RM SF), the prime target elliptical galaxies are those that have large angular sizes and are accessible from the southern hemisphere. Examples include NGC 1316, NGC 3115, NGC 4406, and NGC 5102, all with angular diameters $\approx 10'$ (areas of $\approx$ 0.02 deg^2). Given the amount of RM contribution is expected to be low (Seta et al., 2021), the prospective SKA-Mid observations should be performed

[8] While M 31 is situated in the northern sky, its declination of $\approx +41^\circ$ is still accessible from the SKA.

in Bands 1 and/or 2, with the former being favoured if the Faraday depolarisation effect contributed by the elliptical galaxies is minimal.

With a fiducial integration time of 200 hr per band and per galaxy, the sensitivity that can be attained with the Band 1/2 observations will be 0.17/0.08 μJy/beam, respectively. These will lead to polarised source densities of 540–860 deg^{-2} for Band 1 and 680–890 deg^{-2} for Band 2. With our nominated target elliptical galaxies above (each with $\approx$ 0.02 deg^2 area), we can expect 10–20 background polarised sources behind each of those galaxies. These measurements will place strong constraints on magnetic field properties in ellipticals and on the parameters of the small-scale dynamo theory.

5.3.4 Small-scale Magnetic Fields in Intermediate-redshift Galaxies

The turbulent magnetic field strength on small scales (smaller than the projected size of the background source – usually 10s of pc) can be derived from the $\sigma_{\rm RM}$ difference between the lensed images (with assumptions on the electron density/typical turbulent cell size). We note the importance of higher frequency data (i.e. Bands 3 and 4) in detecting the $\sigma_{\rm RM}$ caused by lensing galaxies. It was shown in Kovacs et al. (2026) that using only L-band data (i.e. 1–2 GHz) can lead to the inability to measure $\sigma_{\rm RM}$ (for the case of the lensing system B1600+434).

The SKA is expected to discover $\approx 10^5$ new lensing systems (see e.g. McKean et al., 2015). With the large sample size, it can become feasible to characterise the outer scale of turbulence (see Kovacs et al., 2026, for detailed discussions). However, we note that the exact technique will still need to be developed and verified with numerical simulation data. Finally, we highlight the significant improvements in the sensitivity using the SKA when compared to, e.g., the VLA. From the work of Kovacs et al. (2026), the on-source integration time was 13 min in L-band (1–2 GHz), 5 min in S-band (2–4 GHz), 9 min in C1-band (4–6 GHz), and 7 min in C2-band (6–8 GHz). Similar exposure time using the SKA-Mid will yield $\approx$ 5 times better sensitivity.

5.3.5 Circumgalactic Medium (CGM) of Low-redshift Galaxies

The statistical studies of the CGM magnetic fields in nearby galaxies have just been enabled with LOFAR (Heesen et al., 2023) and MeerKAT (Böckmann et al., 2023) surveys. While CGM magnetism studies on a per-galaxy basis can be possible for systems within $\approx$ 10 Mpc using on-going surveys such as POSSUM (Gaensler et al., 2025), the analysis of such nearby systems can be challenging. This is because the great angular extents ($\gtrsim$ deg) can lead to difficulties in decoupling between the CGM and the Milky Way ISM contributions to the spatially fluctuating RM. By targeting more distant galaxies that have smaller angular sizes ($\ll$ deg), the Galactic RM fluctuations can be reduced, leading to more accurate characterisation of the magnetic fields in the CGM.

With the SKA-Mid AA4, the direct study of the magnetic fields in the CGM of a large sample of low-redshift ($z \lesssim 0.01$) galaxies can be realised (see also Mao et al. 2026 Chapter for further discussions). In particular, assuming the magnetic halo of the CGM to be about 200 kpc in diameter (Shah and Seta, 2021; Heesen et al., 2023; Shah et al., 2025) and with a target sample size of 20 polarised sources background to the CGM, we will require a polarised source density of 360 deg^{-2} to map the CGM magnetic fields for a galaxy at $z = 0.01$. This translates to a per-galaxy integration time (sen-

sitivity) of 12–60 hr (0.3–0.7 μJy/beam) for Band 1 and 8–30 hr (0.2–0.4 μJy/beam) for Band 2. These figures are reasonable and a Key Science Program sampling a few dozen of such galaxies can be feasible. Alternatively, if one were to dedicate, say, 200 hr of SKA-Mid time on one single galaxy of interest, the resulting source density (sensitivity) will be 560–860 deg^{-2} (0.17 μJy/beam) for Band 1, and 680–890 deg^{-2} (0.08 μJy/beam) for Band 2. Maintaining the constraint of 20 polarised sources within the 200 kpc of the central galaxy as assumed above, the redshift limit will be $z \leq 0.013$–0.016 with Band 1 and $z \leq 0.014$–0.016 with Band 2.

5.4 Synergies beyond Radio

We highlight here a few select advancements beyond the radio regime in recent years / near future that will be highly relevant to the study of small-scale galactic magnetic fields. First of all, the limitations of the many existing thermal electron number density (n_e) models of the Milky Way have been pointed out (e.g. Ocker et al., 2024). Upcoming optical spectroscopic surveys, such as the Local Volume Mapper (LVM; Drory et al., 2024) with the Sloan Digital Sky Survey V (SDSS-V) that will cover sky areas such as the Galactic mid-plane, Orion, and the Magellanic Clouds, will provide high-quality data that will enable improved constraints of n_e. Such information will be highly valuable for galactic magnetism studies via Faraday rotation (both RM and Faraday complexity; e.g. Livingston et al., 2022, 2024; Ma et al., 2025), including the study of the small-scale magnetic fields. Specifically, high-spatial-resolution n_e information will allow one to isolate the small-scale magnetic fields' contribution to spatial RM fluctuations (see e.g. Seta et al., 2023).

Next, the combined analysis between the SKA and data from starlight polarisation surveys (e.g. Magalhães et al., 2012; Tassis et al., 2018; Clemens et al., 2020; Versteeg et al., 2023), with the latter supplemented by accurate distance measurements from e.g. *Gaia* parallax (Luri et al., 2018), holds the prospect of considerable advancements in our knowledge in the small-scale magnetic fields in the Solar neighbourhood (within a few kpc). Recent efforts in conjoining Galactic radio polarised diffuse emission and starlight polarisation data (e.g. Panopoulou et al., 2021; Turić et al., 2021) have highlighted the ability in placing distance constraints to the former. Generalising this, and taking into account that both tracers can offer a tomographic view of the magnetic fields in the local ISM (e.g. Van Eck et al., 2017; Panopoulou et al., 2019; Thomson et al., 2019; Pelgrims et al., 2024), future careful comparisons and combinations of these two powerful magnetic tracers will almost certainly provide us with a clear view of the ISM magnetic fields in our vicinity.

Finally, we point out the recent advents of various 3D maps of the local ISM (within a few kpc), including those of dust extinction (Edenhofer et al., 2024), Hα emission (McCallum et al., 2025), and hydrogen (atomic and molecular) number density (Söding et al., 2025). These are the results of combining the high quality data from various large-scale surveys of the Milky Way ISM with sophisticated analysis and inference algorithms. Apart from the usefulness of these (and the future) 3D maps in aiding our understanding of the small-scale magnetic fields in the Milky Way, we anticipate that future SKA surveys may in turn contribute to next generations of 3D maps of the Milky Way ISM.

6 Summary

In this Chapter, we provide an overview of the prospects of the SKA in advancing our understanding of the small-scale magnetic fields in galaxies, thereby contributing to a better understanding of the fundamental physics of dynamos, as well as the roles that magnetic fields play in star formation and galaxy evolution (Sec. 1 & 4). The most promising tracers of the small-scale galactic magnetic fields that the SKA AA4 will be sensitive to are (i) diffuse synchrotron emission, (ii) rotation measure (RM), (iii) Faraday complexity, and (iv) the Zeeman effect (as summarised in Sec. 2). Combined with upcoming and innovative analysis methods that will be developed using the ongoing polarisation surveys of SKA precursor telescopes (Sec. 5.1), we will characterise and better understand the strength, scale, and structure of the galactic magnetic fields with greater accuracy (Sec. 3).

The general SKA observational requirements for our research field are summarised in Sec. 5.2. We argue that with the SKA-Low, a uniform wide-area polarisation survey, in addition to deep targeted observations of nearby molecular clouds, will be the most fruitful for our science direction. Meanwhile, with the SKA-Mid, wide-area surveys (except for Band 1) appear unlikely to transform our understanding of the subject, given the expected yields of ongoing polarisation surveys such as POSSUM and MMGPS. Instead, we advocate for deep integration (10–1000 hr per pointing) observations of specific sky areas of interest to bring forth a generational leap in our knowledge of astrophysical magnetic fields. We highlight the prospects of SKA-Mid Bands 3 and 4 in studying the extreme Galactic environments (e.g., the Galactic Centre and along the Galactic mid-plane; Sec. 5.2). With this thought, we propose and discuss a few possible large-scale science programs with SKA for deciphering the physics and impact of the small-scale magnetic fields in galaxies (Sec. 5.3).

7 Acknowledgements

We thank Rainer Beck and Tom Landecker for their very useful comments and suggestions on the text. Y. K. M. is partially supported by the Federal Ministry of Education and Research (BMBF) in Germany via the German Academic Exchange Service (DAAD) Project-based Personnel Exchange Programme (PPP). A. S. is supported by the Australian Research Council through the Discovery Early Career Researcher Award (DECRA) Fellowship (project DE250100003) funded by the Australian Government and the Australia-Germany Joint Research Cooperation Scheme of Universities Australia (UA–DAAD, 2025–2026). S. H. acknowledges funding by the European Union (ERC, ISM-FLOW, 101055318). Views and opinions expressed are, however, those of the author(s) only and do not necessarily reflect those of the European Union or the European Research Council. Neither the European Union nor the granting authority can be held responsible for them. M. P. acknowledges the INAF grant 2023 MERCATOR ("MultiwavelEngth signatuRes of Cosmic rAys in sTar-fOrming Regions") and the INAF grant 2024 ENERGIA ("ExploriNg low-Energy cosmic Rays throuGh theoretical InvestigAtions at INAF"). G. P. acknowledges support from the Swedish Research Council (VR) under grant number 2023-04038 and the Knut and Alice Wallenberg Foundation Fellowship program under grant number 2023.0080. L. A. acknowledges support through the Program "Rita Levi Montalcini" of the Italian MIUR. R. M. C. acknowledges support from the Australian Research Council via grant DP230101055 shared with Prof. Mark Krumholz. S. M. acknowl-

edges support from grant PID2023-146372OB-I00, funded by MICIU/AEI/10.13039/501100011033 and by ERDF, EU.

References

A. U. Abeysekara et al. *Science*, 358(6365):911–914, Nov. 2017. doi: 10.1126/science.aan4880.

M. Ackermann et al. *Phys. Rev. D*, 82(9):092004, Nov. 2010. doi: 10.1103/PhysRevD.82.092004.

O. Adriani et al. *Phys. Rev. Let.*, 106(20):201101, May 2011. doi: 10.1103/PhysRevLett.106.201101.

M. Aguilar et al. *Phys. Rev. Let.*, 113(12):121102, Sep 2014. doi: 10.1103/PhysRevLett.113.121102.

M. I. R. Alves, F. Boulanger, K. Ferrière, and L. Montier. *A&A*, 611:L5, Mar. 2018. doi: 10.1051/0004-6361/201832637.

C. S. Anderson, B. M. Gaensler, and I. J. Feain. *ApJ*, 825(1):59, July 2016. doi: 10.3847/0004-637X/825/1/59.

C. S. Anderson et al. *MNRAS*, 533(4):4068–4080, Oct. 2024. doi: 10.1093/mnras/stae1954.

Y. Angarita et al. *AJ*, 168(1):47, July 2024. doi: 10.3847/1538-3881/ad4b14.

L. Baidoo et al. *ApJ*, 955(1):16, Sept. 2023. doi: 10.3847/1538-4357/acebc5.

A. Basu and S. Sur. *Galaxies*, 9(3):62, Sept. 2021. doi: 10.3390/galaxies9030062.

A. Basu et al. *MNRAS*, 464(1):1003–1017, Jan. 2017. doi: 10.1093/mnras/stw2369.

R. Beck. *A&A*, 470(2):539–556, Aug. 2007. doi: 10.1051/0004-6361:20066988.

R. Beck. *A&A*, 578:A93, June 2015. doi: 10.1051/0004-6361/201425572.

R. Beck. *ARA&A*, 24:4, Dec. 2016.

R. Beck and E. M. Berkhuijsen. *A&A*, 700:A198, Aug. 2025. doi: 10.1051/0004-6361/202555048.

R. Beck and M. Krause. *Astron. Nachr.*, 326:414–427, July 2005. doi: 10.1002/asna.200510366.

R. Beck and R. Wielebinski. In T. D. Oswalt and G. Gilmore, editors, *Planets, Stars and Stellar Systems. Vol. 5: Galactic Structure and Stellar Populations*, page 641. Springer, Berlin, 2013.

R. Beck et al. *ARA&A*, 34:155–206, 1996. doi: 10.1146/annurev.astro.34.1.155.

R. Beck, L. Chamandy, E. Elson, and E. G. Blackman. *Galaxies*, 8(1):4, Dec. 2019. doi: 10.3390/galaxies8010004.

H. Beuther et al. *A&A*, 595:A32, Oct. 2016. doi: 10.1051/0004-6361/201629143.

K. Böckmann et al. *A&A*, 678:A56, Oct. 2023. doi: 10.1051/0004-6361/202346777.

A. Bracco et al. *A&A*, 644:L3, Dec. 2020. doi: 10.1051/0004-6361/202039283.

A. Bracco, M. Padovani, and J. D. Soler. *A&A*, 677:L11, Sept. 2023. doi: 10.1051/0004-6361/202347283.

A. Bracco et al. *A&A*, 694:A148, Feb. 2025. doi: 10.1051/0004-6361/202452010.

A. Brandenburg and K. Subramanian. *Phys. Rep.*, 417:1–209, Oct. 2005. doi: 10.1016/j.physrep.2005.06.005.

M. A. Brentjens and A. G. de Bruyn. *A&A*, 441:1217–1228, Oct. 2005. doi: 10.1051/0004-6361:20052990.

B. Burkhart, A. Lazarian, and B. M. Gaensler. *ApJ*, 749:145, Apr. 2012. doi: 10.1088/0004-637X/749/2/145.

B. J. Burn. *MNRAS*, 133:67, Jan. 1966. doi: 10.1093/mnras/133.1.67.

C. J. Cesarsky and H. J. Volk. *A&A*, 70:367, Nov. 1978.
J. Y. H. Chan et al. *MNRAS*, 484(2):1427–1455, Apr. 2019. doi: 10.1093/mnras/sty3498.
J. Y. H. Chan et al. In *Advancing Astrophysics with the SKA – II (AASKAII)*. 2026. arXiv search: Report number AASKAII/Chan01.
B. D. G. Chandran. *ApJ*, 529:513–535, Jan. 2000. doi: 10.1086/308232.
D. P. Clemens et al. *ApJSS*, 249(2):23, Aug. 2020. doi: 10.3847/1538-4365/ab9f30.
R. M. Crutcher et al. *ApJ*, 725(1):466–479, Dec. 2010. doi: 10.1088/0004-637X/725/1/466.
A. C. Cummings et al. *ApJ*, 831:18, Nov. 2016. doi: 10.3847/0004-637X/831/1/18.
A. P. Curtin, J. M. Weisberg, and J. M. Rankin. *ApJ*, 975(2):217, Nov. 2024. doi: 10.3847/1538-4357/ad7b15.
S. Dhakal and A. Seta. *MNRAS*, Oct. 2025. doi: 10.1093/mnras/staf1816.
C. Dickinson et al. In *Advancing Astrophysics with the Square Kilometre Array (AASKA14)*, page 102, Apr. 2015. doi: 10.22323/1.215.0102.
N. Drory et al. *AJ*, 168(5):198, Nov. 2024. doi: 10.3847/1538-3881/ad6de9.
R. Dutta, S. Sur, and A. Basu. *ApJ*, 976(2):168, Dec. 2024. doi: 10.3847/1538-4357/ad891c.
S. Dwivedi, C. Anandavijayan, and P. Bhat. *The Open Journal of Astrophysics*, 7:75, Sept. 2024. doi: 10.33232/001c.122855.
R. P. Eatough et al. *Nature*, 501(7467):391–394, Sept. 2013. doi: 10.1038/nature12499.
G. Edenhofer et al. *A&A*, 685:A82, May 2024. doi: 10.1051/0004-6361/202347628.
B. G. Elmegreen and J. Scalo. *ARA&A*, 42(1):211–273, Sept. 2004. doi: 10.1146/annurev.astro.41.011802.094859.
T. A. Enßlin, S. Hutschenreuter, V. Vacca, and N. Oppermann. *Phys. Rev. D*, 96:043021, Aug 2017. doi: 10.1103/PhysRevD.96.043021. URL https://link.aps.org/doi/10.1103/PhysRevD.96.043021.
A. Erceg et al. *A&A*, 663:A7, July 2022. doi: 10.1051/0004-6361/202142244.
D. Farnsworth, L. Rudnick, and S. Brown. *AJ*, 141(6):191, June 2011. doi: 10.1088/0004-6256/141/6/191.
C. Federrath and R. S. Klessen. *ApJ*, 761(2):156, Dec. 2012. doi: 10.1088/0004-637X/761/2/156.
K. Ferrière, J. L. West, and T. R. Jaffe. *MNRAS*, 507(4):4968–4982, Nov. 2021. doi: 10.1093/mnras/stab1641.
A. Fletcher et al. *MNRAS*, 412:2396–2416, Apr. 2011. doi: 10.1111/j.1365-2966.2010.18065.x.
B. M. Gaensler, R. Beck, and L. Feretti. *New Astron. Rev.*, 48(11-12):1003–1012, Dec. 2004. doi: 10.1016/j.newar.2004.09.003.
B. M. Gaensler et al. *Science*, 307:1610–1612, Mar. 2005. doi: 10.1126/science.1108832.
B. M. Gaensler et al. *Nature*, 478:214–217, Oct. 2011. doi: 10.1038/nature10446.
B. M. Gaensler et al. *PASA*, 42:e091, June 2025. doi: 10.1017/pasa.2025.10031.
S. T. Garrington, J. P. Leahy, R. G. Conway, and R. A. Laing. *Nature*, 331:147–149, Jan. 1988. doi: 10.1038/331147a0.
F. A. Gent et al. *MNRAS*, 432(2):1396–1423, June 2013. doi: 10.1093/mnras/stt560.
F. A. Gent, M.-M. Mac Low, M. J. Korpi-Lagg, and N. K. Singh. *ApJ*, 943(2):176, Feb. 2023. doi: 10.3847/1538-4357/acac20.
J. L. Han. *ARA&A*, 55(1):111–157, Aug. 2017. doi: 10.1146/annurev-astro-091916-055221.
J. L. Han, R. Beck, and E. M. Berkhuijsen. *A&A*, 335:1117–1123, July 1998. doi: 10.48550/arXiv.

astro-ph/9805023.

L. Harvey-Smith, G. J. Madsen, and B. M. Gaensler. *ApJ*, 736(2):83, Aug. 2011. doi: 10.1088/0004-637X/736/2/83.

N. E. Haugen, A. Brandenburg, and W. Dobler. *Phys. Rev. E*, 70(1):016308, July 2004. doi: 10.1103/PhysRevE.70.016308.

M. Haverkorn. In A. Lazarian, E. M. de Gouveia Dal Pino, and C. Melioli, editors, *Magnetic Fields in Diffuse Media*, volume 407 of *Astrophysics and Space Science Library*, page 483, 2015. doi: 10.1007/978-3-662-44625-6_17.

M. Haverkorn et al. *ApJ*, 609(2):776–784, July 2004. doi: 10.1086/421341.

M. Haverkorn et al. *ApJSS*, 167(2):230–238, Dec. 2006. doi: 10.1086/508467.

M. Haverkorn, J. C. Brown, B. M. Gaensler, and N. M. McClure-Griffiths. *ApJ*, 680:362-370, June 2008. doi: 10.1086/587165.

V. Heesen et al. *A&A*, 670:L23, Feb. 2023. doi: 10.1051/0004-6361/202346008.

I. Heywood et al. *ApJ*, 925(2):165, Feb. 2022. doi: 10.3847/1538-4357/ac449a.

S. Hutschenreuter et al. *A&A*, 657:A43, Jan. 2022. doi: 10.1051/0004-6361/202140486.

T. R. Jaffe et al. *MNRAS*, 401(2):1013–1028, Jan. 2010. doi: 10.1111/j.1365-2966.2009.15745.x.

R. Jansson and G. R. Farrar. *ApJL*, 761(1):L11, Dec. 2012. doi: 10.1088/2041-8205/761/1/L11.

A. P. Kazantsev. *Soviet Journal of Experimental and Theoretical Physics*, 26:1031, May 1968.

A. Khadir et al. *ApJ*, 977(2):276, Dec. 2024. doi: 10.3847/1538-4357/ad8ddf.

M. Kierdorf et al. *A&A*, 642:A118, Oct. 2020. doi: 10.1051/0004-6361/202037847.

A. Korochkin, D. Semikoz, and P. Tinyakov. *A&A*, 693:A284, Jan. 2025. doi: 10.1051/0004-6361/202451440.

T. O. Kovacs et al. *A&A*, 705:A28, Jan. 2026. doi: 10.1051/0004-6361/202453502.

M. R. Krumholz and C. Federrath. *Frontiers in Astronomy and Space Sciences*, 6:7, Feb. 2019. doi: 10.3389/fspas.2019.00007.

M. R. Krumholz, B. Burkhart, J. C. Forbes, and R. M. Crocker. *MNRAS*, 477(2):2716–2740, June 2018. doi: 10.1093/mnras/sty852.

R. A. Laing. *MNRAS*, 193:439–449, Nov. 1980. doi: 10.1093/mnras/193.3.439.

R. A. Laing. *Nature*, 331:149–151, Jan. 1988. doi: 10.1038/331149a0.

T. L. Landecker et al. *A&A*, 520:A80, Sept. 2010. doi: 10.1051/0004-6361/200913921.

H.-B. Li et al. *Nature Astronomy*, 1:0158, Aug. 2017. doi: 10.1038/s41550-017-0158.

N. B. Linzer, L. Armillotta, E. C. Ostriker, and E. Quataert. *ApJ*, 988(2):214, Aug. 2025. doi: 10.3847/1538-4357/ade5ad.

R.-Y. Liu, H. Yan, and H. Zhang. *Phys. Rev. Let.*, 123(22):221103, Nov. 2019. doi: 10.1103/PhysRevLett.123.221103.

J. D. Livingston et al. *MNRAS*, 502(3):3814–3828, Apr. 2021. doi: 10.1093/mnras/stab253.

J. D. Livingston et al. *MNRAS*, 510(1):260–275, Feb. 2022. doi: 10.1093/mnras/stab3375.

J. D. Livingston et al. *MNRAS*, 535(2):1944–1963, Dec. 2024. doi: 10.1093/mnras/stae2416.

M. S. Longair. *High Energy Astrophysics*. Feb. 2011.

X. Luri et al. *A&A*, 616:A9, Aug. 2018. doi: 10.1051/0004-6361/201832964.

Y. K. Ma et al. *MNRAS*, 487(3):3432–3453, Aug. 2019. doi: 10.1093/mnras/stz1325.

Y. K. Ma, S. A. Mao, A. Ordog, and J. C. Brown. *MNRAS*, 497(3):3097–3117, Sept. 2020. doi: 10.1093/mnras/staa2105.

Y. K. Ma et al. *MNRAS*, 521(1):60–83, May 2023. doi: 10.1093/mnras/stad462.

Y. K. Ma et al. *MNRAS*, 541(1):306–336, July 2025. doi: 10.1093/mnras/staf1000.

J. P. Macquart and D. B. Melrose. *ApJ*, 545(2):798–806, Dec. 2000. doi: 10.1086/317852.

A. M. Magalhães et al. In J. L. Hoffman, J. Bjorkman, and B. Whitney, editors, *Stellar Polarimetry: from Birth to Death*, volume 1429 of *American Institute of Physics Conference Series*, pages 244–247. AIP, May 2012. doi: 10.1063/1.3701933.

I. Makarenko et al. *Journal of Plasma Physics*, 84(4):735840403, Aug. 2018a. doi: 10.1017/S0022377818000752.

I. Makarenko et al. *MNRAS*, 475(2):1843–1858, Apr. 2018b. doi: 10.1093/mnras/stx3337.

S. Malik and P. Pavaskar. *A&A*, 707:A175, 2026. doi: 10.1051/0004-6361/202553849. URL https://doi.org/10.1051/0004-6361/202553849.

S. Malik, K. H. Yuen, and H. Yan. *MNRAS*, 524(4):6102–6113, Oct. 2023. doi: 10.1093/mnras/stad2225.

S. Malik, K. H. Yuen, and H. Yan. *ApJ*, 965(1):65, Apr. 2024. doi: 10.3847/1538-4357/ad34d7.

S. A. Mao et al. *ApJ*, 688:1029–1049, Dec. 2008. doi: 10.1086/590546.

S. A. Mao et al. *ApJ*, 800(2):92, Feb. 2015. doi: 10.1088/0004-637X/800/2/92.

S. A. Mao et al. *Nature Astronomy*, 1:621–626, Sept. 2017. doi: 10.1038/s41550-017-0218-x.

S. A. Mao et al. In *Advancing Astrophysics with the SKA – II (AASKAII)*. 2026. arXiv search: Report number AASKAII/Mao01.

S. S. Mathew, C. Federrath, and A. Seta. *MNRAS*, 518(4):5190–5214, Feb. 2023. doi: 10.1093/mnras/stac3415.

L. McCallum et al. *MNRAS*, 540(1):L21–L27, June 2025. doi: 10.1093/mnrasl/slaf023.

J. McKean et al. In *Advancing Astrophysics with the Square Kilometre Array (AASKA14)*, page 84, Apr. 2015. doi: 10.22323/1.215.0084.

A. H. Minter and S. R. Spangler. *ApJ*, 458:194, Feb. 1996. doi: 10.1086/176803.

J. S. Morgan et al. *MNRAS*, 473(3):2965–2983, Jan. 2018. doi: 10.1093/mnras/stx2284.

D. Moss and A. Shukurov. *MNRAS*, 279:229–239, Mar. 1996. doi: 10.1093/mnras/279.1.229.

S. K. Ocker et al. *ApJ*, 974(1):10, Oct. 2024. doi: 10.3847/1538-4357/ad6a51.

A. Y. L. On et al. *MNRAS*, 490(2):1697–1713, Dec. 2019. doi: 10.1093/mnras/stz2683.

T. J. O'Neill et al. *ApJ*, 988(2):191, Aug. 2025. doi: 10.3847/1538-4357/ade306.

S. P. O'Sullivan et al. *MNRAS*, 421(4):3300–3315, Apr. 2012. doi: 10.1111/j.1365-2966.2012.20554.x.

S. P. O'Sullivan et al. *MNRAS*, 469(4):4034–4062, Aug. 2017. doi: 10.1093/mnras/stx1133.

S. P. O'Sullivan et al. *MNRAS*, 519(4):5723–5742, Mar. 2023. doi: 10.1093/mnras/stac3820.

S. P. O'Sullivan et al. In *Advancing Astrophysics with the SKA – II (AASKAII)*. 2026. arXiv search: Report number AASKAII/OSullivan01.

P. V. Padmanabh et al. *MNRAS*, 524(1):1291–1315, Sept. 2023. doi: 10.1093/mnras/stad1900.

M. Padovani and D. Galli. *A&A*, 620:L4, Nov. 2018. doi: 10.1051/0004-6361/201834222.

M. Padovani, D. Galli, and A. E. Glassgold. *A&A*, 501:619–631, July 2009. doi: 10.1051/0004-6361/200911794.

M. Padovani, A. V. Ivlev, D. Galli, and P. Caselli. *A&A*, 614:A111, June 2018. doi: 10.1051/0004-6361/201732202.

M. Padovani et al. *A&A*, 651:A116, June 2021. doi: 10.1051/0004-6361/202140799.

A. Pandhi et al. *ApJ*, 968(2):50, June 2024. doi: 10.3847/1538-4357/ad40aa.

A. Pandya, Z. Zhang, M. Chandra, and C. F. Gammie. *ApJ*, 822(1):34, May 2016. doi: 10.3847/0004-637X/822/1/34.

G. V. Panopoulou et al. *ApJ*, 872(1):56, Feb. 2019. doi: 10.3847/1538-4357/aafdb2.

G. V. Panopoulou et al. *ApJ*, 922(2):210, Dec. 2021. doi: 10.3847/1538-4357/ac273f.

G. V. Panopoulou et al. *A&A*, 694:A97, Feb. 2025. doi: 10.1051/0004-6361/202450991.

D. Paré et al. *ApJ*, 969(2):150, July 2024. doi: 10.3847/1538-4357/ad4462.

K. Pattle et al. In S. Inutsuka et al., editors, *Protostars and Planets VII*, volume 534 of *Astronomical Society of the Pacific Conference Series*, page 193, July 2023. doi: 10.48550/arXiv.2203.11179.

V. Pelgrims et al. *A&A*, 684:A162, Apr. 2024. doi: 10.1051/0004-6361/202349015.

S. Piras et al. *A&A*, 687:A267, July 2024. doi: 10.1051/0004-6361/202349085.

Planck Collaboration et al. *A&A*, 586:A138, Feb. 2016. doi: 10.1051/0004-6361/201525896.

Planck Collaboration et al. *A&A*, 586:A136, Feb. 2016. doi: 10.1051/0004-6361/201425305.

S. B. Ponnada et al. *MNRAS*, 527(4):11707–11718, Feb. 2024. doi: 10.1093/mnras/stad3978.

N. K. Porayko et al. *MNRAS*, 483(3):4100–4113, Mar. 2019. doi: 10.1093/mnras/sty3324.

S. Ranchod et al. *A&A*, 686:A104, June 2024. doi: 10.1051/0004-6361/202348993.

N. C. Raycheva et al. *A&A*, 663:A170, July 2022. doi: 10.1051/0004-6361/202039474.

F. Rincon. *Journal of Plasma Physics*, 85(4):205850401, Aug 2019. doi: 10.1017/S0022377819000539.

T. Robishaw et al. In *Advancing Astrophysics with the Square Kilometre Array (AASKA14)*, page 110, Apr. 2015. doi: 10.22323/1.215.0110.

T. Robishaw et al. In *Advancing Astrophysics with the SKA – II (AASKAII)*. 2026. arXiv search: Report number AASKAII/Robishaw01.

L. Rudnick and F. N. Owen. *ApJ*, 785(1):45, Apr. 2014. doi: 10.1088/0004-637X/785/1/45.

M. Ruszkowski and C. Pfrommer. *A&ARv*, 31(1):4, Dec. 2023. doi: 10.1007/s00159-023-00149-2.

A. A. Ruzmaikin, D. D. Sokoloff, and A. M. Shukurov, editors. *Magnetic fields of galaxies*, volume 133 of *Astrophysics and Space Science Library*, 1988. doi: 10.1007/978-94-009-2835-0.

G. B. Rybicki and A. P. Lightman. *Radiative processes in astrophysics*. 1979.

A. A. Schekochihin. *Journal of Plasma Physics*, 88(5):155880501, Oct. 2022. doi: 10.1017/S0022377822000721.

A. A. Schekochihin et al. *New Journal of Physics*, 4:84, Oct. 2002. doi: 10.1088/1367-2630/4/1/384.

A. A. Schekochihin et al. *ApJ*, 612:276–307, Sept. 2004. doi: 10.1086/422547.

D. H. F. M. Schnitzeler. *MNRAS*, 409(1):L99–L103, Nov. 2010. doi: 10.1111/j.1745-3933.2010.00957.x.

A. Seta and R. Beck. *Galaxies*, 7(2):45, Apr 2019. doi: 10.3390/galaxies7020045.

A. Seta and C. Federrath. *MNRAS*, 499(2):2076–2086, Sept. 2020. doi: 10.1093/mnras/staa2978.

A. Seta and C. Federrath. *Physical Review Fluids*, 6(10):103701, Oct. 2021. doi: 10.1103/PhysRevFluids.6.103701.

A. Seta and C. Federrath. *MNRAS*, 514(1):957–976, July 2022. doi: 10.1093/mnras/stac1400.

A. Seta and C. Federrath. *MNRAS*, 533(2):1875–1886, Sept. 2024. doi: 10.1093/mnras/stae1935.

A. Seta and N. M. McClure-Griffiths. *MNRAS*, 539(2):1024–1039, May 2025. doi: 10.1093/mnras/staf520.

A. Seta et al. *MNRAS*, 473:4544–4557, Feb. 2018. doi: 10.1093/mnras/stx2606.

A. Seta, P. J. Bushby, A. Shukurov, and T. S. Wood. *Phys. Rev. Fluids*, 5:043702, Apr 2020. doi: 10.1103/PhysRevFluids.5.043702. URL https://link.aps.org/doi/10.1103/PhysRevFluids.5.043702.

A. Seta, L. F. S. Rodrigues, C. Federrath, and C. A. Hales. *ApJ*, 907(1):2, Jan. 2021. doi: 10.3847/1538-4357/abd2bb.

A. Seta, C. Federrath, J. D. Livingston, and N. M. McClure-Griffiths. *MNRAS*, 518(1):919–944, Jan. 2023. doi: 10.1093/mnras/stac2972.

H. Shah and A. Seta. *MNRAS*, 508(1):1371–1388, Nov. 2021. doi: 10.1093/mnras/stab2500.

H. Shah, F. van de Voort, A. Seta, and C. Federrath. *MNRAS*, 541(3):2471–2492, Aug. 2025. doi: 10.1093/mnras/staf1066.

R. Shanahan et al. *ApJL*, 887(1):L7, Dec. 2019. doi: 10.3847/2041-8213/ab58d4.

T. W. Shimwell et al. *A&A*, 659:A1, Mar. 2022. doi: 10.1051/0004-6361/202142484.

A. Shukurov and K. Subramanian. *Astrophysical Magnetic Fields: From Galaxies to the Early Universe*. Cambridge Astrophysics. Cambridge University Press, 2021.

K. Silsbee, A. V. Ivlev, M. Padovani, and P. Caselli. *ApJ*, 863(2):188, Aug. 2018. doi: 10.3847/1538-4357/aad3cf.

C. Sobey et al. *MNRAS*, 484(3):3646–3664, Apr. 2019. doi: 10.1093/mnras/stz214.

C. Sobey et al. *MNRAS*, 504(1):228–247, June 2021. doi: 10.1093/mnras/stab861.

L. Söding et al. *A&A*, 693:A139, Jan. 2025. doi: 10.1051/0004-6361/202451361.

D. D. Sokoloff et al. *MNRAS*, 299:189–206, Aug. 1998. doi: 10.1046/j.1365-8711.1998.01782.x.

T. Sprenger et al. *MNRAS*, 515(4):6198–6216, Oct. 2022. doi: 10.1093/mnras/stac2160.

J. M. Stil, A. R. Taylor, and C. Sunstrum. *ApJ*, 726(1):4, Jan. 2011. doi: 10.1088/0004-637X/726/1/4.

E. C. Stone, A. C. Cummings, B. C. Heikkila, and N. Lal. *Nature Astronomy*, 3:1013–1018, Nov. 2019. doi: 10.1038/s41550-019-0928-3.

R. A. Stutz, E. W. Rosolowsky, R. Kothes, and T. L. Landecker. *ApJ*, 787(1):34, May 2014. doi: 10.1088/0004-637X/787/1/34.

K. Subramanian. *MNRAS*, 294:718–728, Mar. 1998. doi: 10.1046/j.1365-8711.1998.01284.x10.1111/j.1365-8711.1998.01284.x.

K. Subramanian. *Reports on Progress in Physics*, 79(7):076901, July 2016. doi: 10.1088/0034-4885/79/7/076901.

X. Sun et al. In *Advancing Astrophysics with the SKA – II (AASKAII)*. 2026. arXiv search: Report number AASKAII/Sun01.

S. Sur and K. Subramanian. *MNRAS*, 527(2):3968–3981, Jan. 2024. doi: 10.1093/mnras/stad3535.

M. Tahani et al. In *Advancing Astrophysics with the SKA – II (AASKAII)*. 2026. arXiv search: Report number AASKAII/Tahani01.

K. Takayanagi. *PASJ*, 25:327, 1973.

K. Tassis et al. *arXiv e-prints*, art. arXiv:1810.05652, Oct. 2018. doi: 10.48550/arXiv.1810.05652.

A. R. Taylor et al. *AJ*, 125(6):3145–3164, June 2003. doi: 10.1086/375301.

A. J. M. Thomson et al. *MNRAS*, 479(4):5620–5637, Oct. 2018. doi: 10.1093/mnras/sty1865.

A. J. M. Thomson et al. *MNRAS*, 487(4):4751–4767, Aug. 2019. doi: 10.1093/mnras/stz1438.

A. J. M. Thomson et al. *PASA*, 40:e040, Aug. 2023. doi: 10.1017/pasa.2023.38.

A. J. M. Thomson et al. *PASA*, in press. doi: 10.48550/arXiv.2605.16917.

A. Tritsis. *A&A*, 700:A152, Aug. 2025. doi: 10.1051/0004-6361/202554422.

L. Turić et al. *A&A*, 654:A5, Oct. 2021. doi: 10.1051/0004-6361/202141071.

C. L. Van Eck et al. *A&A*, 597:A98, Jan. 2017. doi: 10.1051/0004-6361/201629707.

C. L. Van Eck et al. *A&A*, 623:A71, Mar. 2019. doi: 10.1051/0004-6361/201834777.

C. L. Van Eck et al. *ApJSS*, 283:28, Jan. 2026. doi: 10.3847/1538-4365/ae3dea.

S. Vanderwoude et al. *AJ*, 167(5):226, May 2024. doi: 10.3847/1538-3881/ad2fc8.

M. J. F. Versteeg et al. *AJ*, 165(3):87, Mar. 2023. doi: 10.3847/1538-3881/aca8fd.

C. Wang, J. L. Han, and D. Lai. *MNRAS*, 417(2):1183–1191, Oct. 2011. doi: 10.1111/j.1365-2966.2011.19333.x.

S. L. Wilkin, C. F. Barenghi, and A. Shukurov. *Phys. Rev. Let.*, 99(13):134501, Sept. 2007. doi: 10.1103/PhysRevLett.99.134501.

M. Wolleben and W. Reich. *A&A*, 427:537–548, Nov. 2004. doi: 10.1051/0004-6361:20040561.

M. Xue et al. *PASA*, 34:e070, Dec. 2017. doi: 10.1017/pasa.2017.66.

F. Yusef-Zadeh et al. *ApJL*, 925(2):L18, Feb. 2022. doi: 10.3847/2041-8213/ac4802.

S. Zaroubi et al. *MNRAS*, 454:L46–L50, Nov. 2015. doi: 10.1093/mnrasl/slv123.

Ya. B. Zel'dovich, S. A. Molchanov, A. A. Ruzmaikin, and D. D. Sokoloff. *Soviet Physics Uspekhi*, 30(5):353, 1987.

Table 1: Expected linear polarisation performance of SKA-Low and SKA-Mid AA4

	SKA-Low	SKA-Mid					
		Band 1	Band 2	Band 3	Band 4	Band 5a	Band 5b
Frequency (MHz)	50–350	350–1050	950–1760	1650–3050	2800–5180	4600–8500	8300–15400
RMTF FWHM (rad m^{-2})[a]	0.1	4.8	51	140	420	1200	3700
RM uncertainty (rad m^{-2})[a,b]	0.008	0.4	4	12	35	95	311
RM max-scale (rad m^{-2})[a]	4	38	108	325	937	2522	8278
Angular resolution (arcsec)[c]	9.1	1.3	0.8	0.4	0.2	0.1	0.08
Image rms noise (1 hr; μJy/beam)[c]	7.0	2.3	1.1	?	?	0.7	0.8
Pol src density (1 hr; deg^{-2})[d,e]	1–10?	80–130	100–130	?	?	70–90	50–60

[a]: Following Eq. 61 and 62 of Brentjens and de Bruyn (2005).

[b]: Evaluated at a linear polarisation signal-to-noise ratio of 6.

[c]: Using Briggs weighting with robust = 0, without *uv*-tapering.

[d]: Estimated using Rudnick and Owen (2014), extrapolated across frequency assuming a spectral index of −0.7.

[e]: See https://github.com/jackieykma/SKA-pol-density, for a script estimating the polarised source density.